Advanced Composites and Hybrid Materials (2019) 2:626–656
https://doi.org/10.1007/s42114-019-00126-3

REVIEW

Advances in transition metal oxide catalysts for carbon monoxide oxidation: a review

Subhashish Dey[1] · Ganesh Chandra Dhal[1] · Devendra Mohan[1] · Ram Prasad[2]

Received: 27 June 2019 / Revised: 14 September 2019 / Accepted: 30 September 2019 / Published online: 5 December 2019

Abstract

The transition metal catalysts have much concerned over the last two to three decades due to their different properties from their bulk-counterparts, which cover the way for their application in various fields. It has shown superior efficiency in selectivity, performances, and stability to the heterogeneous catalysis. Carbon monoxide (CO) is a very harmful gas that exists in the atmosphere and ambient-temperature complete oxidation of it is an important process for human health protection. The performances of transition metal catalysts are highly dependent on the crystallite size, surface area, and pore volume of the catalysts. The chemisorptions of CO over transitional metal and supported catalysts were studied in this review. The transition metal catalysts have been represented an excellent catalyst from lower cost, thermally, activity, and selectivity point of view. This investigation will show scientific basis for potential design of transition metal oxide catalysts for CO oxidation.

Keywords Carbon monoxide · Transition metal · Catalyst · Chemisorptions · Mechanism · Applications

1 Introduction

The catalytic converter applications in an automobile vehicle were used for reducing the poisonous gases emissions from an internal combustion engine. The catalysts which exist in a catalytic converter were a reduction catalyst and an oxidation catalyst [1, 2]. In all situations, the catalysts exist in a ceramic monolith structure and covered with metal support. The catalytic reaction is the reaction between catalyst surfaces and other gases present in the vehicle exhaust [3]. The activity of catalytic converter is strongly depending on the different types of catalysts were applied. In the presence of catalyst, the rate of chemical reaction was improved; it acts like an agent that decreases the activation energy of the reactions. The transition metals, noble metals, and metal oxide are broadly applied as catalyst in a catalytic converter [4, 5].

Carbon monoxide (CO) is very dangerous gas and also represents as the silent killer. CO is produced into the atmosphere by partial oxidation of carbon-containing compounds. It is a neutral and nonirritating gas which makes it very difficult for humans to identify [6, 7]. The low-temperature catalytic conversion of CO is highly important process for life support in enclosed atmospheres such as submarines and spacecraft. Due to the rising cost of noble metals and outstanding performances in oxide preparation, catalytic conversion of CO over transition metal oxide catalysts is currently of much interest, still if several oxides are recognized to present an outstanding performance since the start of the twentieth century [8]. The transition metal oxides (TMOs) constructions, buildings, designing, and structures have been represented as one of the most important useful elements in the area of catalysis, fuel cells, energy storage, air pollution control, and so on. These materials structured units frequently possess certain physical and chemical properties that are especially helpful for their efficient applications [9, 10].

The TMOs catalysts are novel types of mixed oxide catalyst whose exterior surface area chemistry can be considered in the similar situation as effective oxide catalysts [11]. There are different synthesis methods that have been developed for the production of TMOs catalyst with distinctive structure and higher activity [12]. It has a cheaper cost, environmentally friendly, and simply available catalyst for ambient temperature CO conversion. The TMOs catalysts are synthesized via various methods and had been reported to often produce some

✉ Subhashish Dey
subhasdey633@gmail.com

[1] Department of Civil Engineering, IIT (BHU), Varanasi, India

[2] Department of Chemical Engineering and Technology, IIT (BHU), Varanasi, India

small/nanostructures with attractive shapes, such as spherical, pyramids, laminated-cube, and dumbbell structures [13, 14]. The mixed transition metal oxide (MTMOs) catalysts observed from various transition metals should be the new types of candidates due to their prospective application in catalysis and energy exchange [15]. The current research investigated that the structure, characterization, activity, and applications of various transition metal oxides oxide catalysts for CO oxidation [16]. It is very complex species making with oxygen, during the presence of cations; therefore, the characterizations of supported transition metal oxides catalysts are very difficult. The transition metal oxides have superior potential for reduction of CO in the atmosphere so that it is mostly used in a catalytic converter [17, 18].

Transition metal oxides represents huge structural differences due to their capacity to produced phases of different metal to oxygen ratios showing several steady oxidation states of the metal ions. The performances of most active transition metal oxides, such as Co_3O_4, CuOx, Ni_2O_4, ZnOx, or MnOx, are highly dependent on the reaction conditions [19]. Transition metal oxides exhibit high crystallographic anisotropy which may explain the various catalytic properties for various uncovered crystal faces. The surface structures mainly depend upon various strong metal-oxygen bonds at different surface planes [20]. The superior metal-oxygen bond is made more crucial by its function in CO oxidation. The real metal-oxygen stoichiometry and defect structure participate a significant role in partial oxidation reactions [21, 22].

Transition metal oxides contain a large amount of surface structures which involve the surface energy of compounds and affects their chemical properties. It contained oxygen atoms bound to transition metals [23]. The surface metal oxides are highly influenced by the coordination of metal cation and oxygen anion, which modify the catalytic activity of these compounds. The structural defects in TMO are highly influence by their catalytic performances. The location of surface ions will change from the massive structure [24]. In all the transition metal oxides, Mn_2O_3, CuO, ZnO, TiO_2, Fe_2O_3, NiO, and Co_3O_4 show better catalytic performance in CO oxidation [25]. The oxidation state of MnOx is highly affected when applied with MnOx as a support. The certain oxidation state of Mn represents to perform as a reducing agent or oxidizing agent. The oxygen-containing ability in the crystalline lattice and capacity of Mn to create oxides with different oxidation states are its catalytic property [26]. The TiO_2 has more oxygen-containing capacity with superior oxygen adsorption and oxide reduction rates, which can be applied to decrease the amount of CO in the exhaust gases. The titanium oxide can represent superior performances per unit surface region than the individual one of noble metal catalysts [27]. The Co_3O_4 is a unique spinel-structure transition metal oxide catalyst with applications in various fields. The Co_3O_4 as catalysts of environmental implication includes complete oxidation for CO and HC oxidation and NO and SO_2 reduction at a low temperature [28].

Cobalt-based catalyst is sometimes applied in place of noble metals due to its lower cost, high availability, and more activity for complete conversion of CO. Co_3O_4 is the strongly active catalyst in TMO for CO oxidation and represents unusual activity and stability under low temperature in dry conditions [29, 30]. Zinc oxide (ZnO) catalyzes more oxygen available for CO oxidation process. ZnO acts as a reducible oxide support, improving the catalytic performances via metal-support interface and/or better spreading of active metal components [31]. An important property of zinc is its ability to stabilize the catalyst against deactivation due to more thermal constancy and/or superior distribution of active metal. In place of using ZnO individual as the catalyst for CO oxidation, more scientists focus on changing ZnO with various ions to improve their performances and thermal stability [32]. Copper oxide is originally lesser active for CO conversion, but in combination with Mn-oxide in certain proportions, several different active catalytic systems were produced [33]. CuMnOx catalyst is more active in the amorphous state still at room temperature where crystallization of the spinel $CuMn_2O_4$ phase has occurred. In high oxygen-rich environmental conditions, the affirmation of oxidation of CuO and reduction of MnO phases in the oxygen-deficient conditions occur, to create residual Cu_2O and $Mn^{2+/3+}$ oxide phases [34, 35].

The iron oxide (Fe_2O_3) catalyst showed a good CO oxidation activity, even at room temperature and it is a potential substitute for precious metal catalysts system. The isolated tetrahedral coordinated Fe(3+) centers have a more catalytic performance in CO oxidation. The existence of Fe^{2+} or Fe^{3+} ion has been recognized as individual one of the major factors governing the structure property of Fe-containing products [36]. The superior activity of iron nanoparticles in CO oxidation was associated with a smaller particle size, higher exterior area, and closely occupied surface coordination unsaturated sites. The iron phase species formed during the activation depends on the time of exposure to the reactant feed, mixture of the feed, and pretreatment conditions [37–39]. The noble metals are highly applied in an automobile vehicle as a catalytic converter. In the noble metal catalysts, rhodium is used as a reduction catalyst, palladium (Pd) is used as an oxidation catalyst, and platinum (Pt) is used for both the reduction and oxidation catalyst. The Pt-, Pd-, and Rh-based catalysts are mostly used for ambient temperature CO oxidation process [39–41].

Gold (Au) is very active for ambient-temperature oxidations of CO if dispersed on suitable metal oxides and complex oxides. Gold supported on reducible oxides represents to catalyze the CO conversion well at the low temperatures over 0 °C. The addition of gold into the catalyst improved their catalytic performances for CO oxidation [42]. It has been reported for high thermal stability mostly due to the substantially

reduced gold-gold nanoparticle interactions. The introduction of gold will add new active sites into the catalysts and also increases the reducibility of the catalyst. An increase of Au^0/Au^{+3} ratio has also been reported when increasing the calcination temperature. An excess of Au^0 is detrimental for CO oxidation [43]. Silver (AgO, Ag_2O, Ag_2O_3)-based catalyst is represented as an attractive metal oxide catalysts and more activity and thermal stability for ambient temperature CO conversion. The performances of silver catalysts are mostly dependent upon their surface structure and composition [44]. The activity of AgO catalyst is most commonly as a consequence of the occurrence of different Ag–O interactions. The surface and subsurface oxygen atoms are represented to be the active sites for Ag-based catalysts in CO oxidation reactions. The oxygen pretreatment at high temperature results in the formation of subsurface oxygen and activates silver catalysts Ag^0 as an active species was observed to increase the catalytic activity at a low temperature [45].

Nickel is the best catalyst for the reaction of virtue of its life, high activity, and selectivity toward CO oxidation at a cheaper cost. The high performances of Ni were associated to the existence of both intra- and inter-particle porosity of the catalysts and high Ni metal particles dispersion on the catalyst surfaces. The NiO has a bimodal pore structure; this represents huge performances for CO oxidation [46]. This bimodal pore structure will provide more favorable pore size for the chemisorptions of reactants. The potential of chemisorptions on nickel has transitional binding energies; therefore, it has an intermediate value of the heat adsorption. It is a lower cost, active, and best catalyst to be produced economically. The performance of catalysts also depends upon the calcination conditions of precursors and subsequent pretreatment of the catalysts [47]. This review paper mainly focused on the low-cost transition metal catalysts. The influence of particle size on catalytic activity has been subjected of continuous interest due to its importance from both primary and practical viewpoints [48]. Future studies will focus on the development and utilization of transition metal catalysts for high catalyst selectivity. The catalytic activity of various transition metal catalysts in different compositions in CO oxidation reactions has been discussed in this review paper.

2 Chemistry of carbon monoxide

Carbon monoxide contains single C atom, and a single O atom consisted of a triple bond that has two covalent bonds and one dative covalent bond. This is the easiest oxo-carbon. In coordination complexes, the CO ligand is called carbonyl. CO is a molecule with three resonance structures or Lewis structure. It can clarify the outstanding adsorption properties and reactivity of this molecule on oxide and metal surfaces. CO is one of the strongest diatomic molecules and a weak electron donor. In the structure with three covalent bonds, the octet rule was satisfied, but the electropositive carbon has a negative charge [44]. Calculations with usual bond orbital exposed that the structure through the triple bond is the most significant. This is following other theoretical and experimental studies that represent the superior electro-negativity of oxygen dipole moment points from the negative carbon end to the positive oxygen end [49].

3 Property and structure of various transition metal oxide catalysts

The transition metal oxides are composed of oxygen atoms bound to transition metals. It is frequently applied for their catalytic performances and semi-conductive properties. TMO have a broad range of surface structures which influence the surface energy of these compounds and affects their physical-chemical properties. The surface metal oxides are also influenced by the allocation of metal cation and oxygen anion, which influences the catalytic activity of these compounds [46, 47]. The structural defects in TMO are highly affected by their catalytic properties. The surface structure of transition metal oxides catalysts is bulk crystalline in nature. The oxide crystal structure is depending upon on close-pack arrangement of oxygen anions, with metal cations covering interstitial sites. The close-packed arrays, such as face-centered-cubic (fcc) and hexagonal close-packed (hcp), have both octahedral and tetrahedral interstices. In mono-oxide, many TMO (TiO and NiO) have rocksalt structure. In rocksalt structure, the octahedral sites have cations in an oxygen anion fcc array [44]. The majority of TMO (MO_2; M = Ti, Cr, V, Mn, Zr, Pd, etc.) have the rutile structure. The rutile structure is produced by filling half of the octahedral sites with cations of the hcp oxygen anion array. In trioxides, few TMO can reach to the +6 oxidation state. The mixture of two or more metals in an oxide form produces a huge number of structures [47–49]. The ternary oxide may be influenced by changing the proportions of two components and their (SrV_2O_6 and Sr_2VO_4) oxidation states. The perovskite structure is commonly observed in transition metal oxides produced with one big (A) and one small cation (B). In this structure, a cubic array of B cations with the A cations occupying the center of cube and oxide atoms are located at the center of 12 edges of plain cube [50]. The bond between oxygen and transition metal as shown in Fig. 1 is strongly affected by the coordination of metal cations and oxygen anions as well as the filling of metal in d-orbitals. The surface coordination is illicit by the face that is exposed in the surface reduction [51].

The catalytic properties of perovskite-type oxides mainly depend on the nature of A and B ions and their valence state. The nature of these ions also influences the stability of

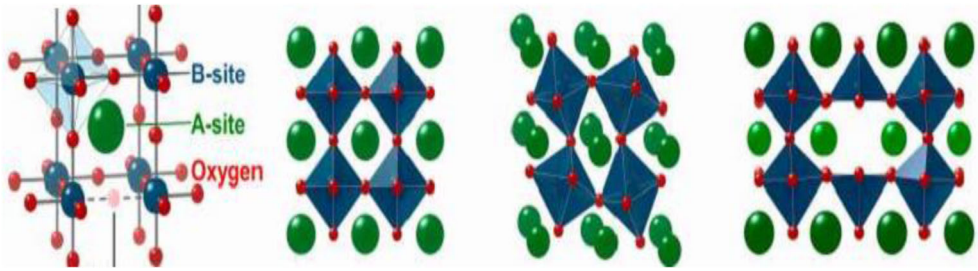

Fig. 1 Molecular structure of transitional metal oxides in perovskite catalysts

perovskite phase. Many TMOs are highly active for CO oxidation without utilizing noble metal [52]. The two key factors usually establish the efficiency of TMOs for CO oxidation, reducibility, and oxygen mobility. In these reactions, the CO reduces a dynamic metal center. The oxygen mobility in the transition metal oxides lattice, as shown in the Fig. 2, corresponds to improved oxygen vacancies at the exterior surface to adsorb active oxygen and extra reactive lattice oxygen [53].

The character of cobalt oxides mainly in the proportion of Co^{2+}, Co^{3+}, and Co^{4+} was mostly applied for CO oxidation. In all the presence of cobalt oxide, the most active form would be Co_3O_4 in which cobalt is observed in two valence states (+2 and +3). The crystal structure of Co_3O_4 as shown in Fig. 3 is a perfect spinel structure in which Co^{2+} cations occupy one-eighth of the tetrahedral sites while Co^{3+} cations occupy half of the octahedral sites. The spinel Co_3O_4 is also the most stable oxide [52].

In comparison to Co_3O_4, the unsupported CuO have been rarely used in CO oxidation. This is necessary due to the distinctive structure of Co_3O_4, which contains both Co^{2+} and Co^{3+}, whereas CuO or Cu_2O have only either Cu^{2+} or Cu^{+} ions [53]. However, CuO are not highly stable as shown in the Fig. 4 and oxidation state of Cu may fluctuate in the course of reaction. Depending on the CO/O_2 ratio and temperature, it very much depend on Cu^{2+} and Cu^{+} that coexist, despite of the first materials. The outstanding behavior of Cu_2O in CO oxidation at room temperature observed in detail is the O_2 chemisorptions on the cuprous oxide.

The manganese oxide nanoparticles are prepared by self-assembly in a single pot reaction in ambient conditions with interesting morphologies and high surface areas. Manganese oxide catalysts are steady in the presence of Mn_2O_3, MnO_2, and Mn_3O_4 phases which were mostly dependent on the calcination temperature between 200 and 300 °C [54]. The labile oxidation state represents Mn to act either as a reducing agent or oxidizing agent. The oxygen contains ability in the crystalline lattice and capacity of Mn to produce oxides with different oxidation states determines its catalytic property [55]. The structure of manganese oxide catalysts is shown in Fig. 5 and represents huge amount of necessary work dedicated to instruct the role played by each element and nature of active sites [56].

The isolated tetrahedral coordinated Fe(3+) centers and phases of $FeMnO_2$ are recognized as structural applications for high catalytic performances in the CO oxidation. Iron is usually played as the active metal in the catalyst for industrial scale due to their economically acceptable cost. The oxide of Fe^{2+} as shown in Fig. 6 was consisting of (FeO and FeO_2) and oxides of Fe^{2+} and Fe^{3+} were consisting of (Fe_3O_4, Fe_4O_5, Fe_5O_6, Fe_5O_7, $Fe_{25}O_{32}$, and $Fe_{13}O_{19}$) oxides. The oxide of Fe^{3+} was consisting of Fe_2O_3. The metallic iron (Fe^0) peaks present in the iron oxide precursor before calcination [57].

The nickel oxide (NiO) also represents an active phase for CO oxidation when deposited on the catalyst surfaces. The NiO was produced and highly dispersed on catalyst surface, resulting in the production of rich surface Ni^{2+} ions. The Ni^{2+} ions moderately replace Mn^{3+}/Mn^{4+} ions to produced a Ni–Mn solid solution and creating surface oxygen vacancies, which are crucial for CO oxidation. The Ni and Mn have same electronic configurations, which possible expected results in the Ni–Mn composite oxides capable to synergistic catalytic effect [46]. The oxidation of metallic alloys are shown in the Fig. 7 containing Ni, which can be expected to yield strong interaction of Ni and support oxides with high dispersion. The sub and full monolayer of oxygen chemisorbed over Ni surfaces play no significant role in low-temperature CO oxidation

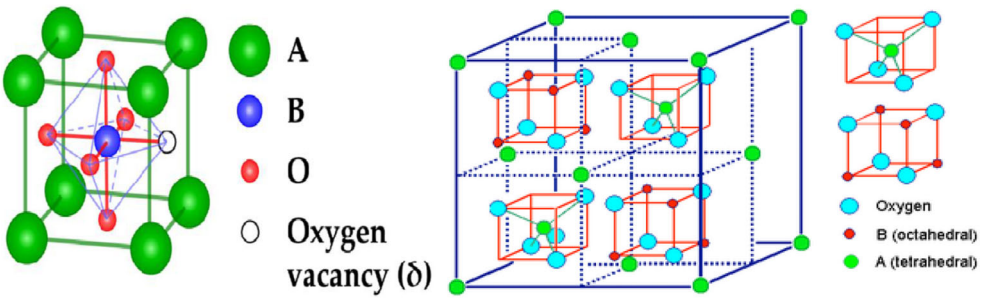

Fig. 2 Oxygen position in various transition meal oxide catalysts

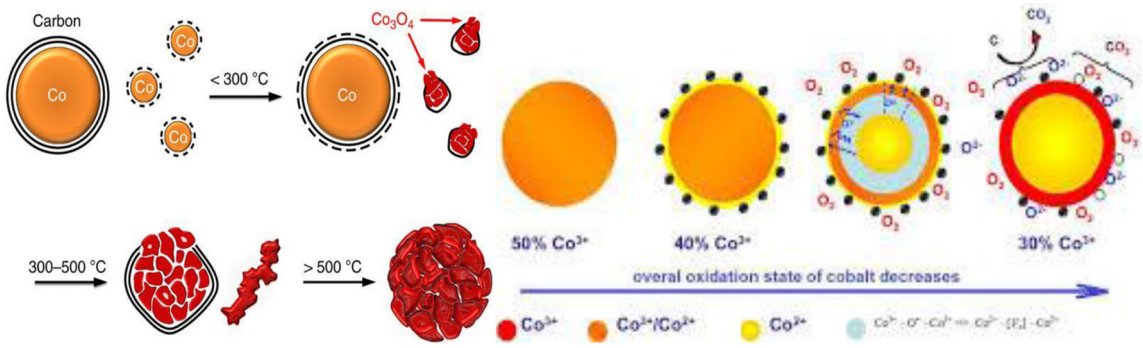

Fig. 3 Formation of various cobalt nanoparticles

process but NiO can catalyze the low-temperature CO oxidation when NiO was saturated by O_2. The NiO cubic phase was thermo stable and stop changing phase has occurred [58].

Titania is sometimes used for CO conversion processes although can be an outstanding support for certain metals, mainly gold. The highly dispersed Ir/TiO_2 catalysts represent huge catalytic activity for CO oxidation even at room temperature, similar to that of size-selected supported Au nanoparticles [27]. Titanium dioxide is a naturally occurring oxide of titanium (TiO_2). TiO_2 represents in nature as the recognized raw materials like rutile, anatase, and brookite. Molten TiO_2 has a simple structure in which each Ti is coordinated to, on average, about 5 oxygen atoms and crystalline produced in which Ti coordinates to 6 oxygen atoms [59].

Nanosized TiO_2 is shown in the Fig. 8, the small size represents high catalytic activity. This activity is apparently distinct at the {001} planes and even though the {101} planes are thermodynamically further stable structure. The TiO_2 in thin film and nanoparticle form is probable applied in energy production [27–29]. The TiO_2 was applied as different support materials for heterogeneous catalyst due to the consequence of its huge textural area stabilizing the catalysts in its mesopores structure. Among all the transition metal oxide additives, zinc oxide (ZnO) was used as promoter to increase the catalytic performances of gold catalysts for partial oxidation of methanol and CO oxidation. The Au-ZnO/Al_2O_3 catalyst is further active than the Au/Al_2O_3 catalyst, where smaller particles led to higher activities [32].

The zinc oxide crystallites are mainly found in dual forms hexagonal wurtzite and cubic zincblende. The wurtzite structure is highly stable at ambient conditions. The zincblended produces can be stabilized by increasing ZnO on substrates with cubic lattice structure. In these cases, the zinc and oxide centers are tetrahedral, the majority characteristic geometry for Zn(II). Nanostructures of ZnO as shown in Fig. 9 can be prepared in different morphologies including nanowires, nanorods, tetrapods, nanobelts, nanoflowers, nanoparticles, etc [60]. The novel metal catalysts are very helpful in CO oxidation processes. These catalysts are very dense, expensive relatively rare earth metal. The rate of CO dissociation will strongly depend on the particle size and geometry of surface assembly involved in the dissociation reaction. The CO adsorbs only on (111) and (001) surface planes as compared with stepped sites, where CO dissociates with low barrier. The energy barrier for CO dissociation is higher than the desorption energy for CO oxidation [61].

4 Chemisorptions of carbon monoxide over transition metal oxide catalysts

Several groups have been considered for CO conversion over different catalysts since they have significance in environmental protections. Catalytic performances for CO oxidation mostly depend upon the metal ion concentration on the surface and surface crystalline. Carbon dioxide is formed by the reaction of CO with oxygen adsorbed on the metal ions of

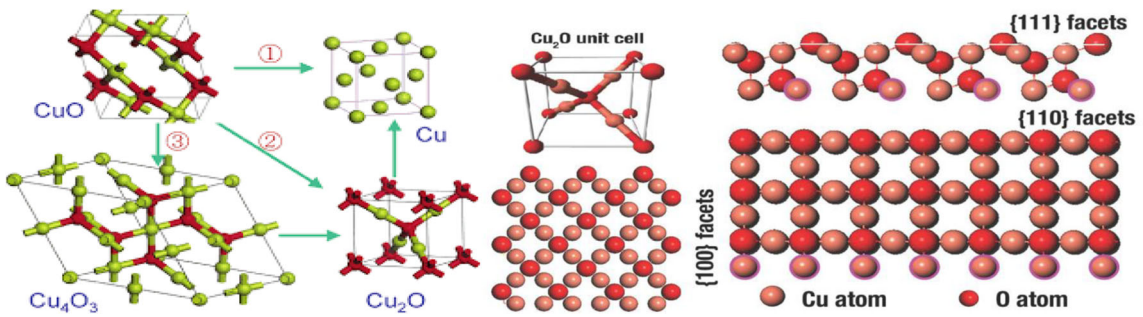

Fig. 4 Structure of Cu and O atoms in copper oxide catalysts

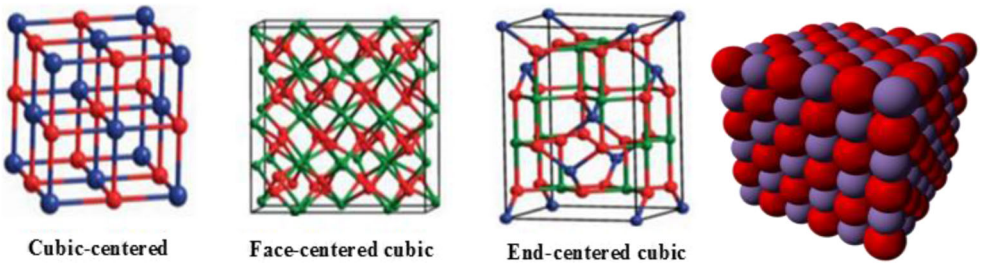

Fig. 5 Structure of different manganese oxide catalysts

outmost surface. A surface concentration of oxygen was monitored for subsequent reaction and partial pressures of reactants [62]. Co_3O_4 has perfect spinel structure in which one-eighth of the tetrahedral sites are covered by Co^{2+} cations while half of the octahedral sites are covered by Co^{3+} cations. Co_3O_4 is essentially active for CO oxidation even under a temperature of − 54 °C. The pure Co^{III} oxide was used in CO oxidation as a starting material and Co_3O_4 instinctively loses oxygen to give CoO.

High activity which originates from Co_3O_4 {110} facets has been described in Fig. 10 to the improvement of octahedral coordinated Co^{3+} cations which represent best CO chemisorptions properties and poorer barriers for reaction between adsorbed CO and oxygen. The adsorption of CO on the surface of cobalt oxide is demonstrated in Table 1 that Co ions mostly originate over the surface of Co_3O_4 {111} and Co_3O_4 {100} thin films or synthetically produced on the CoO {111} surface are very essential for chemical properties of the surface [61]. The Cu_2O catalyst is highly active at low temperature and catalyst system composition of Cu_2O nanoparticles supported on silica gel that exhibited exceptional activity toward CO oxidation. The oxygen species associated with Cu in the Cu_2O catalyst are highly active and mostly dominated by the ambient conditions CO conversion. In oxygen-rich atmospheric conditions, the presence of reduced copper oxide to produce residual Cu_2O oxide phase was noted. The Cu_2O catalyst is very much active in amorphous state at ambient conditions but has been observed to lose their performances after exposition at high temperatures [63]. The CuO particles minor than (< 3 nm) are well isolated in the oxide matrix, to start with, and after the reaction. The advanced loading rate of CuO supports can lead to create bigger size nanoparticles; it is the main reason for lowering the activity. At the increasing temperature, the oxidation of CO proceeded fastest over Cu, followed by Cu^+ and Cu^{2+}, in order of rising oxidation state. High density of active sites on the catalyst exterior surfaces is present therefore its performances increase [63]. The reaction of Cu and CuO whereas a redox mechanism would preferentially be done over Cu_2O which oscillates between Cu(II) and Cu(I) during the CO oxidation process. The Cu^+ cations situated at the exterior surface of grain boundaries as shown in the Fig. 11 would be the most dynamic sites for CO conversion at low temperature as discussed in Table 2. The Cu_2O catalyst is highly active in O_2-rich than in O_2-lean conditions [62, 63].

The CO was chemisorb on six different sites of Cu_2O catalyst surface and disperse fast over O sites. The reduced species of copper (Cu^0, Cu+) are essential for better CO conversion but lower size copper particles could be lesser active than higher ones [64]. In all transition metal oxides, the Mn_2O_3 represents superior catalytic activity in CO oxidation. The reaction of Mn_2O_3 and O_2 producing MnO_2 is affected by oxygen concentration and temperature. The increasing oxygen concentration and lower temperature are more beneficial to the production of MnO_2 [65].

The lower oxygen concentration and increasing temperatures are slower the generation of MnO_2 and Mn_2O_3 as the reaction proceed. The manganese oxide catalysts as shown in the Fig. 12 have more activities per unit surface area than those of noble metal catalysts. The Mn_2O_3 applied to be the major active oxide, falling at the lowest temperature. The oxidation state of manganese continuously moves between Mn^{4+} and Mn^{3+} [66, 67]. The titanium oxide increased

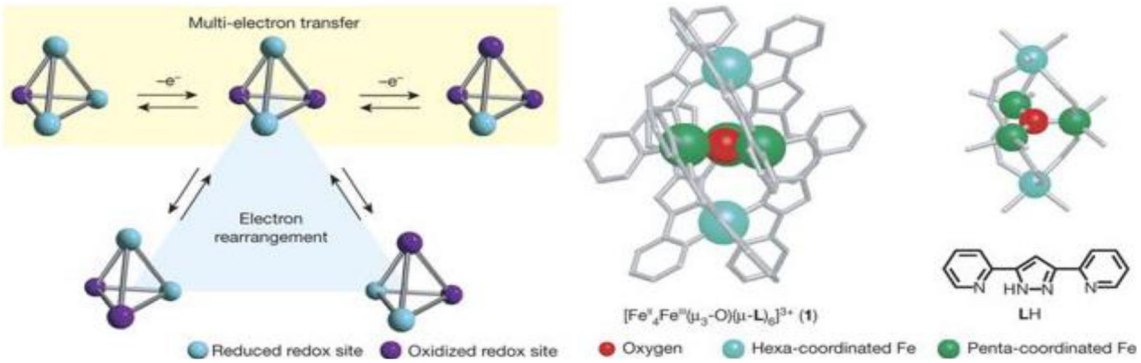

Fig. 6 Structure of iron oxide catalysts

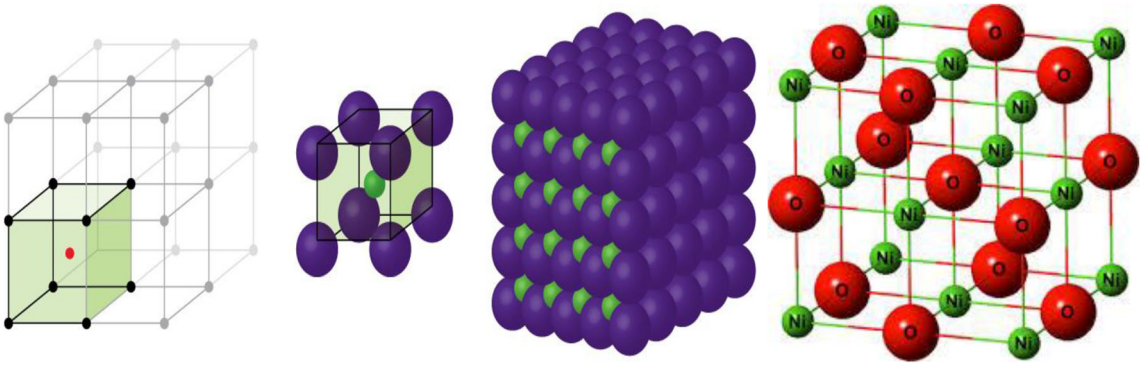

Fig. 7 Structure of nickel oxide catalysts

performances toward partial oxidation of CO, but had an opposite effect in the case of non-stoichiometric TiO_x. The oxygen vacancies increased by the conductivity of TiO_x film [27].

The CO conversion activities over a series of TiO_2-supported catalysts and activity order observed as $Co/TiO_2 > Cu/TiO_2 > Mn/TiO_2 > Ni/TiO_2 > V/TiO_2 > Cr/TiO_2 > Fe/TiO_2$. The Co/TiO_2 exhibits the best activity and 100% CO conversion, as shown in the Fig. 13, was obtained at temperatures below 15 °C [27, 59]. The Ir/TiO_2 catalyst also shows good performance for CO oxidation. Iron is single one of the major active catalysts for CO oxidation. The moderate performances of Fe_2O_3 are more significant than the Fe_3O_4 catalysts. The performances of different Fe oxides catalysts were discussed in Table 3 as follows: $Fe_3O_4 < Fe_2O_3$. The Fe_2O_3 is most active iron oxide catalysts for CO conversion [68].

The unsupported and supported Fe_2O_3, as shown in the Fig. 14, are highly active for CO conversion. The authors reported the following order of activity in CO conversion: $Fe_2O_3/Al_2O_3 > Fe_2O_3/TiO_2 \approx Fe_2O_3 > FeSbO_4 > FePO_4 > Fe_2(MoO_4)_3$. A hexagonal close-packed structure in all of the Fe^{3+} ions in octahedral sites is noted. The octahedral sites are empty and can be packed by Fe^{2+} ions to produce magnetite Fe_3O_4. The Fe species can be stabilized in porous materials such as graphene or gamma-alumina [69]. After the Fe-C bond formation, a serious step of CO oxidation reaction participates one terminal Fe-O bond activation, and rate-determining step is O-O bond activation. In the presence of reduced cationic species of Fe, still metallic iron atoms would be very significant in the reaction mechanism, whereas over oxidized iron sites would be very active in the catalytic process [70]. Promotion of $CuO/MnO_2–Al_2O_3$ by nickel may improve the catalytic performances and stability of CuMn–alumina catalysts. The NiO does not represent better activity in CO conversion as shown in the Fig. 15, compared to cobalt and copper oxides [58].

The activity of CuO is improved constantly by nickel accumulation resultants to a reduction in copper oxide dispersion. Although, a pure perovskite phase is obtained with crystal structure and cell parameter changed with nickel inclusion. The chemisorptions of CO over nickel at (111) faces were higher than copper and cobalt [46, 47]. The zinc oxide catalysts are important for the conversion of CO gas. The copper zinc oxides are highly active catalysts for the conversion of CO at ambient temperature. Pure ZnO is active at 200 °C in the catalysis oxidation of CO. Oxygen species appears to be adsorbed in an ionic as well as a non-ionic form, while CO and CO_2 are adsorbed essentially in non-ionic forms [32].

Two surface sites, may be Zn^+ ions, are shown in Fig. 16, necessary to attach O_2 and CO_2. Carbon dioxide is not an inhibitor in the reaction but common displacement of CO_2 and O_2 was shown. The kinetic study of CO oxidation shows that the O_2 was adsorbed weakly and CO strongly on two different types sites of ZnO catalysts. The amount of ionic species O^-(ads) nearly does not fluctuate on the exterior of ZnO, the order ½ with respect to oxygen is interpreted as participating in the reaction of non-ionic oxygen O(ads) [60].

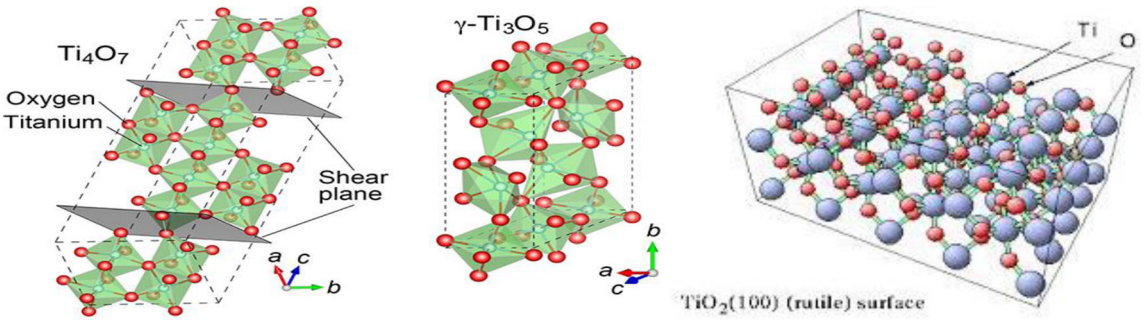

Fig. 8 Various structures of titanium oxide catalysts

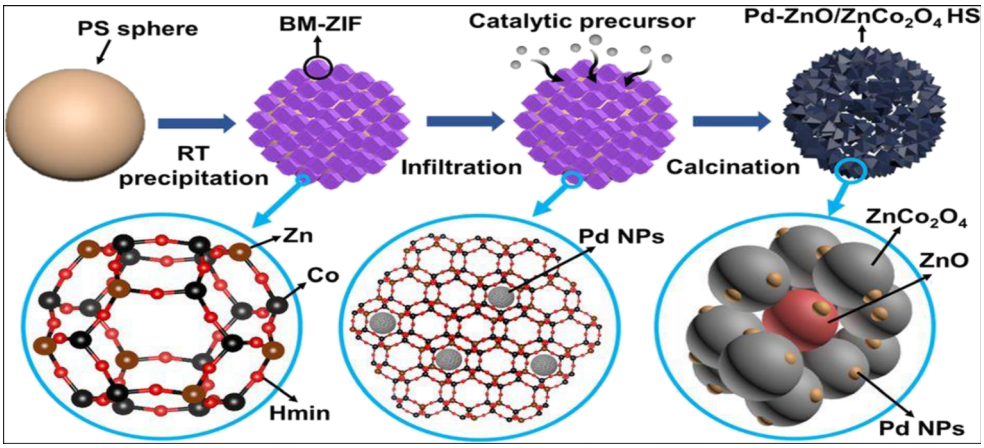

Fig. 9 Structural formation of zinc oxide after calcination

The electron exchange between Cu and Cr leads to the reserve of reduction in Cu-Cr catalysts and thus Cu is the major dynamic species for CO conversion. The catalysts performances were related with the production of various Cu-Cr species such as $CuCr_2O_4$ and $Cu_2Cr_2O_4$. In Cu-Cr system, the dual types of active centers present on the catalyst surface [71]. The CO conversion rises with the increasing of Cr content in the active component. The rate of CO conversion passes all over highest at (15–30%) Cr content after which fast decreases. The involvement of Cu species with Cr species results to a superior CO conversion as shown in Fig. 17 because of the high synergistic effect in the Cu-Cr/γ–alumina catalysts. This catalyst is active when the metal particles are in metallic form, and agglomeration to bigger particles as well as oxidation decreases the activity. The noble metals (Pt, Pd, Rh, Ru, Ag, and Au) continuing price rise stimulated an increasing substitution by other low cost elements [72, 73]. The performance of supported catalyst is strongly affected by the volume and texture of metal species as discussed in Tables 4, 5, 6, 7, and 8. The performance of iridium species on supports for CO conversion can be measured on molecular concepts [74]. The iridium supported on TiO_2 synthesized by the deposition-precipitation method was more active for CO oxidation than Ir/Al_2O_3 and Ir/Fe_2O_3 catalysts [75].

To catalyze the conversion of dry CO over Ir/rutile, catalysts initiated their catalytic performances over 50 °C, while Au/rutile and Ir-Au/rutile catalysts were very active for this reaction under ambient temperature. The Ir/TiO_2 is very active than Ir/SnO_2, Ir/Al_2O_3, and Ir/Fe_2O_3 catalysts toward CO oxidation [76]. The small crystallites size depends on Ir and was highly constant due to IrO_2 having the similar crystalline. The lanthanum perovskite catalysts showed that great catalytic performances for CO oxidation at the higher temperatures. Lanthanum is oxidized in the form of various La oxide catalysts with fine metallic particles of La produced in a radius of 1–3 nm [77]. The improvement of catalytic performances for conversion of CO over La catalysts, in association with La catalysts, could be a certain result due to mixing of La and Co in the small particles [78]. Alumina initially combine with Co_3O_4 can represent to the cobalt oxide as a superior thermal resistance can improve its performances. The $Co_3O_4/\gamma\text{-}Al_2O_3$ is very active catalyst for CO oxidation at low temperature. This single-atom catalyst has enormously more atomic efficiency and represents high activity and stability for CO conversion [79]. The CO conversion activity over distinct ferrites, say $NiFe_2O_4$, $CoFe_2O_4$, and $CuFe_2O_4$, is in the order $NiFe_2O_4 < CoFe_2O_4 < CuFe_2O_4$ which is in superior contact. The performances and selectivity of catalysts depend on the contact between individual components, for which a uniform distribution of components all through the material without definite separation is a pre-requisite [80].

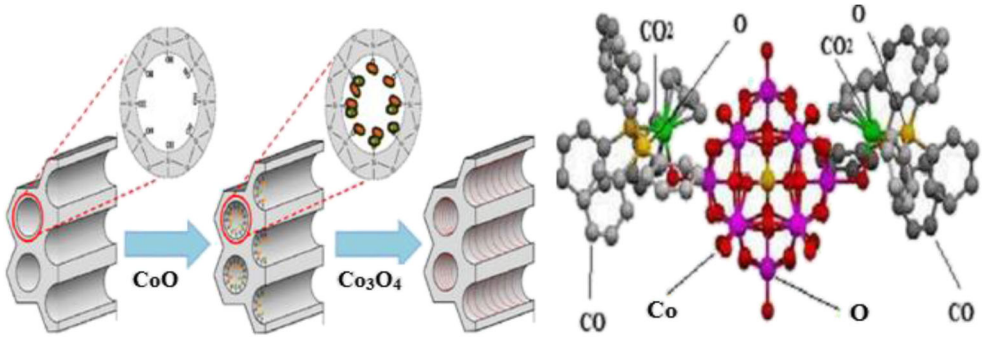

Fig. 10 Structural bonding between cobalt oxide and carbon monoxide

Table 1 The operating parameters and activity measurement of cobalt oxide catalysts for CO conversion

Catalyst	Preparation method	Operating parameters	Remarks	References
Co_3O_4 nanorods	Precipitation method	The gas composition of 1 vol% CO, 2.5 vol% O_2/He and feed rate 3.91×10^{-6} mol g^{-1} S^{-1} under dry conditions	Co_3O_4 nanorods (T_i = − 63 °C, T_{50} = 23 °C, T_{100} = 77 °C)	Xie et al. 2005 [22]
Co_3O_4 Au-Co_3O_4	Co-precipitation method	The Au particle dia. 5 nm, specific surface area 52.1 m^2/g, weight 300 mg, flow rate 20,000 h^{-1}.ml/g-cat, size distribution 70–120 mesh. The gases contains 1% CO, 99% air at 200 °C for 40 min	Co_3O_4 (T_i = 30 °C, T_{50} = 48 °C, T_{100} = 60 °C) Au-Co_3O_4 (T_i = − 85 °C, T_{50} = − 70 °C, T_{100} = − 55 °C)	Cunningham et al. 1994 [28]
Co_3O_4	Liquid phase precipitation method	The 300 mg catalyst under feed gases 0.5 vol% CO, 14.4 vol% O_2, and 85.1 vol% N_2 with a complete flow rate 20 ml/min	Co_3O_4 (T_{100} = 25°C Time = 50 min)	Wang et al. 2008 [30]
Mesoporous Co_3O_4	Nanocasting pathway	The 200 mg catalyst with mixture of 0.5 vol% CO, 16.4 vol% O_2, and 83.4 vol% N_2 at flow rate of 20 ml/min to SV 4000 ml g-cat^{-1} h^{-1}.	Mesoporous Co_3O_4 (T_i = − 4 °C, T_{50} = 40 °C, T_{100} = 82 °C)	Tuysuz et al. 2008 [31]
Co_3O_4	Precipitation method	The 5 mg catalyst exposed by the gas mixture for 2 min rate of 100 ml.min^{-1} (1.0% CO, 1.0% O_2, rest is air)	Co_3O_4 (T_i = 70 °C, T_{50} = 160 °C, T_{100} = 220 °C)	Grillo et al. 2004 [48]
Cobalt Metal oxides	Impregnation method	The 100 mg catalyst with flow rate: 20 cm^3 min^{-1} of 1% CO in Ar stoichiometric ratio: S = 2[O_2]/[CO] at 22 °C for 70 min	Co_3O_4 (T_i = 40 °C, T_{50} = 90 °C, T_{100} = 120 °C) CoOx/SiO_2 (T_i = 200 °C, T_{50} = 300 °C, T_{100} = 450 °C) Au/CoOx/SiO_2 (T_{50} = 10 °C, T_{100} = 90 °C) $LaCoO_3$ (T_i = 100 °C, T_{50} = 220 °C, T_{100} = 300 °C) $La_{1-x}Ba_xCoO_3$ (T_i = 80 °C, T_{50} = 100 °C, T_{100} = 120 °C)	Royer and Duprez 2011 [33]
Cobalt-based catalyst	Co-precipitation method	The 25–35 mg catalyst with total flow velocity 25 ml/min and reactant gases are 1(vol%) CO, 21(vol%)O_2, and He. Temp. in range of 20–200 °C at time 90 min	Co_3O_4 (T_i = 120 °C, T_{50} = 180 °C, T_{100} = 240 °C)	Balikci and Gulder 2007 [11]
Cobalt oxide	Incipient wetness impregnation method	The 50 mg catalyst with H_2/CO/N_2 = 12:6:2 and GHSV = 1200 h^{-1}	Cobalt oxide CeO_2 > TiO_2 > ZrO_2 (Xco = 35% at R.T.)	Kraum and Baerns 1999 [49]
CoO nanoparticles	Colloidal dispersing method	The 50 mg catalyst with gas composition of CO_2 sccm and compacted dry air 20 sccm. The heating rate 2 °C/min and time 90 min	CoO nanoparticles (T_{100} = 110 °C)	Mankidy et al. 2014 [52]
CoOx	Precipitation-oxidation method	The 40 mg catalyst with reactant gas (10% O_2/He with 4% Co/He) on stream flow rate 25 ml/min. The reactor temp. increased from 28 to 200 °C for 1 h	CoOx (T_i = 20 °C, T_{50} = 80 °C, T_{100} = 140 °C)	Lin et al. 2003 [53]
Mesoporous Co-Fe-O nanocatalyst	Precipitation method	The 200 mg catalyst consisting of 10 vol% CO balanced with air. The entire flow velocity was 36.5 ml/min and WHSV	Mesoporous Co-Fe-O (T_i = 60 °C, T_{50} = 75 °C, T_{100} = 140 °C)	Cao et. al. 2014 [39]

Table 1 (continued)

Catalyst	Preparation method	Operating parameters	Remarks	References
		was 11,000 ml/h/g		
Co_3O_4	Self-consistent	The 50 mg catalyst in a gas composition of 1 vol% CO in air (1 vol% CO, 19.8 vol% O_2, balanced with N_2). The complete flow rate was 50 ml/min and increase at a temp. rate of 2 °C/min	Co_3O_4 (T_i = 15 °C, T_{50} = 75 °C, T_{100} = 140 °C)	Deng et al. 2015 [67]
Co_3O_4	Impregnation method	The 50 mg catalyst with a reactant gases of 1.0 vol% CO in air. The entire gases flow rate was 100 ml/min and GHSV was 120,000 ml h^{-1} g_{cat}^{-1}	Co_3O_4 (T_i = 35 °C, T_{50} = 65 °C, T_{100} = 115 °C)	Sun et al. 2010 [70]
Co-Fe mixed oxide	Conventional Co-precipitation method	The catalyst in presence of 1% CO, 2% O_2, 50% H_2, and balanced He. The total gases flow velocity was 20–40 ml/min, and GHSV was 12,000–24,000 h^{-1}	Co-Fe (Ti = 30 °C, T_{50} = 45 °C, T_{100} = 120 °C) 2Co-Fe (Ti = 15 °C, T_{50} = 25 °C, T_{100} = 85 °C)	Qwabe et al. 2015 [73]
CoO(OH) Co_3O_4	Aqueous precipitation method	The 50 mg catalyst with volumetric flow rate of 1.63 cm^3/s. The inlet gas consists of 0.85% CO + 25% O_2 in Ar. The catalyst heating rate 150 °C/h	Co_3O_4 (T_i = 30 °C, T_{50} = 65 °C, T_{100} = 85 °C) CoO(OH) (T_i = 40 °C, T_{50} = 145 °C, T_{100} = 165 °C)	Salek et al. 2014 [74]
Co_3O_4	Precipitation method	The 100 mg catalyst with gases mixture of 12% H_2, 2% CO, 4% O_2, rest in N_2. The complete flow velocity was 150 cm^3/min	Co_3O_4 (T_i = 90 °C, T_{50} = 165 °C, T_{100} = 240 °C)	Pollard et al. 2008 [82]
Co_3O_4	Incipient wetness method	The 350 mg catalyst with a gas composition of 0.5–5% CO, 0.5–10% O_2 in He. The total gases flow rate was 200 ml/min and GHSV was 24,000 h^{-1}	Co_3O_4 (T_i = 72 °C, T_{50} = 120 °C, T_{100} = 180 °C) Co_3O_4/TiO_2 (T_i = 32 °C, T_{50} = 62 °C, T_{100} = 98 °C)	Kim and Kim 2011 [79]
Co/ZrO_2	Impregnation method	The 200 mg catalyst with feed gas composition CO, O_2, and He. Total flow rate 45 cm^3/min and GHSV was 35,000 h^{-1}	Co/ZrO_2 (T_i = 75 °C, T_{50} = 105 °C, T_{100} = 130 °C)	Yung et al. 2007 [80]
Co_3O_4 nanowires	Thermal decomposition method	The 100 mg (0.25 cm dia.) Co_3O_4 nanowires with inlet gas mixture of 2.7% CO, 8.3% O_2, and 89% N_2. The entire flow velocity was 30 ml/min	Co_3O_4 nanowires (T_i = 80 °C, T_{50} = 130 °C, T_{100} = 160 °C)	Zhang et al. 2009 [84]
Hollow sphere Co_3O_4	Dispersion method	The 10 mg catalyst with feed gas 1.0% CO and 0.5% O_2 in N_2 with complete flow rate of 40 ml/min	Hollow sphere Co_3O_4 (T_i = 20 °C, T_{50} = 87 °C, T_{100} = 170 °C)	Umegaki et al. 2016 [87]
Mesoporous MnO_2 and Co_3O_4	Nanocasting method	The 0.1 gm catalyst with total flow velocity 100 ml/min and SV was 60,000 ml/(gh). The inlet gas consist of 1% CO + O_2 + He (balance) and molar ratio of CO/O_2 = 1/1	MnO_2 (T_i = 60 °C, T_{50} = 200 °C, T_{100} = 270 °C) Mesoporous MnO_2 (T_i = 40 °C, T_{50} = 130 °C, T_{100} = 190 °C) Co_3O_4 (T_i = 50 °C, T_{50} = 150 °C, T_{100} = 240 °C) Mesoporous Co_3O_4 (T_i = 40 °C, T_{50} = 85 °C, T_{100} = 150 °C)	Du et al. 2012 [89]
$Mn_{0.75}Co_{2.25}O_4$	Co-precipitation method	The 150 mg catalyst with flow velocity 100 ml/min and GHSV was 60,000 h^{-1}. A mixed gas	$Mn_{0.75}Co_{2.25}O_4$ (T_i = 25 °C, T_{50} = 60 °C, T_{100} = 95 °C)	Wang et al. 2014 [95]

Table 1 (continued)

Catalyst	Preparation method	Operating parameters	Remarks	References
		stream of 500 ppm CO/21 vol% O_2/N_2 (0–90%) relative humidity		
Co_3O_4-N-CNFs	Nanocomposition method	The 100 mg catalyst with gases composition 0.2 vol% CO, 1.0 vol% O_2, 0.5 vol% Ne/He at a total flow velocity of 1000 cm^3/min and GHSV was 240,000 h^{-1}	Co_3O_4-N-CNFs (T_i = 75 °C, T_{50} = 100 °C, T_{100} = 125 °C)	Podyachea et al. 2014 [96]
Fe-Co nanoparticles	Co-precipitation method	The 100 mg catalyst with inlet gases mixture of 2% CO, 20% O_2, and 10% N_2 balanced He. The total flow velocity was 60 ml/min and GHSV was 60,000 ml/gh	Fe-Co nanoparticles (T_i = 30 °C, T_{50} = 86 °C, T_{100} = 200 °C)	Biabani-Ravandi et al. 2013 [98]
Cobalt support carbon nanotubes	Incipient wetness impregnation method	The 60 mg catalyst at a flow rate of 100 ml/min. The feed gas composition of 1.0% CO, 2.0% O_2, 60% H_2, and He as balanced. The GHSV was 50,000 h^{-1}	Co nanoparticle support carbon nanotubes (T_i = 280 °C, T_{40} = 410 °C Const.)	Lv et al. 2011 [99]
Mesoporous Co_3O_4	Precipitation & hydrothermal methods	The 80 mg catalyst in a reactor with a feed gas composition of 3.4% CO and 21% O_2 balanced He at a complete flow velocity of 42 ml/min	Mesoporous Co_3O_4 rods (T_i = − 115 °C, T_{50} = − 80 °C, T_{100} = − 65 °C) Mesoporous Co_3O_4 wires (T_i = − 90 °C, T_{50} = − 40 °C, T_{100} = − 30 °C) Mesoporous Co_3O_4 mix (T_i = − 70 °C, T_{50} = − 20 °C, T_{100} = 20 °C)	Alvarez et al. 2012 [101]
Co_3O_4	Precipitation method	The 150 mg catalyst with reaction gases consists of 1% CO in air with entire flow velocity of 50 ml/min and SV was 20000 ml/(h·g)	Co_3O_4 (T_i = 40 °C, T_{50} = 90 °C, T_{100} = 110 °C)	Yunbo et al. 2013 [103]
Co_3O_4	Combustion synthesis method	The 75 mg catalyst with 2.4 vol% CO, 11.4 vol% air, and balanced N_2. The total flow velocity was 30 ml/min and space velocity was 47,750 h^{-1}	Co_3O_4 without O_2 (T_i = 220 °C, T_{50} = 280 °C, T_{100} = 350 °C) Co_3O_4 (T_i = 50 °C, T_{50} = 110 °C, T_{100} = 150 °C)	Singh and Madras 2015 [145]
Co_3O_4 nanorods	Precipitation method	The 200 mg catalyst with entire flow velocity of 50 ml/min in presence of 1% CO, 2.5% O_2 balanced He	Co_3O_4 nano rods (T_{100} = − 77 °C)	Xie et al. 2005 [22]
CoOx	Precipitation-oxidation method	The 40 mg catalyst with gas composition of 4% CO/He and 10% O_2/He and entire flow rate was 25 ml/min	CoOx (T_i = 30 °C, T_{50} = 80 °C, T_{100} = 135 °C)	Lin et al. 2003 [53]
Co-Mn-O/FeOx	Deposition-precipitation method	The 200 mg catalyst with 1 vol% CO, 1 vol% O_2, 50 vol% H_2 balanced Ar and GHSV was 15,000 ml/gh	Co-Mn-O/FeOx (T_i = 20 °C, T_{50} = 50 °C, T_{100} = 80 °C)	Zhao et al. 2014 [116]
Co_3O_4/Al_2O_3	After calcination mixing	The reaction gases consists of 2% CO and different concentration O_2, and reaction was performed at 21–50 °C temperature	Co_3O_4/Al_2O_3 (Ti = 28 °C, T_{50} = 80 °C, T_{100} = 215 °C)	Jansson 2000 [24]
Co_3O_4/Al_2O_3	Impregnating method	The gases used are O_2, H_2, CO_2, CO and 6% $18O_2$ in Ar, total sample was used	Co_3O_4/Al_2O_3 (Ti = 12 °C, T_{50} = 45 °C, T_{100} = 57 °C) Nanosized Fe_2O_3	Jansson 2001 [23]

Table 1 (continued)

Catalyst	Preparation method	Operating parameters	Remarks	References
		68 ± 2.2 mg with entire flow velocity of 20 Nml/min, temp. 21 °C		
Cobalt-aluminum oxides	Co-precipitation method	The 100 mg catalyst 250–350 μm size at feed rate 1% CO and 20% O_2 in He was applied (55 Nml/min) increasing up to temperature with 5 K min^{-1} up to 573 K	Co–Al_2O_3 (T_i = 60 °C, T_{50} = 124 °C, T_{100} = 177 °C)	Bordoloi et al. 2014 [61]
CoMo-Al_2O_3	Self-supported	The 500 mg catalyst with entire flow velocity of 100 ml/min, P = 2 MPa, Temp. = 523 K, $P_{(CO)}$ = 1.3 kPa	CoMo-Al_2O_3 (T_i = 35 °C, T_{50} = 65 °C, T_{100} = 110 °C)	Pelardy et al. 2016 [64]
Co-Cr-Al-O	Self-propagating high-temperature synthesis method	The 100 mg catalyst with 1% CO in air at a space velocity 2000 h^{-1}	Co-Cr-Al-O (T_i = 80 °C, T_{50} = 155 °C, T_{100} = 210 °C)	Tyurkin et al. 1997 [100]
CoOx/Al_2O_3	Deposition oxidation–precipitation method	The 50 mg catalyst with CO concentration 0.5%, 9.5% O_2, 52% He, and 38% Ar with entirety flow velocity of 35.5 ml/min. The GHSV was 30,000 ml g^{-1} h^{-1}	CoOx/Al_2O_3 (T_i = 45 °C, T_{50} = 150 °C Const.)	Konova et al. 2006 [105]

5 Mechanism of CO oxidation over transitional metal oxide catalysts

The efficiency of transitional metal catalysts for reactions with CO molecules is strongly depending on the chemisorptions process. The chemisorptions of CO gases are significant step, which increses the concentration of reactant over the catalyst exterior surfaces which chemisorbed on the CO molecules applying on more energy to be simply obtain the chemical reactions. The distinct reaction mechanisms are stable with the observed kinetics. The initial mechanism represents that the highly accepted CO conversion reaction on catalyst exterior surface that participates the O_2 adsorption to produced O_2* precursors, which divide on a vicinal vacancy [81]. In the second mechanism, O_2 activation done via the kinetically applicable with CO*-assisted O_2 dissociation step lacking of the definite conditions of stable O_2* precursors. In the CO conversion procedure, the oxygen was initially adsorbed on catalyst exterior surfaces with the energy of activation. The mechanism of transition metal catalysts for reaction with the CO molecule is shown in the Fig. 18. When the temperature is increase in a certain amount so that the adsorption of oxygen reaches on suitable proportions, therefore any CO passing over the catalyst surfaces either react directly adsorbed oxygen or initially adsorbed then reacts, after which the CO being produced was desorbed.

The performance of transitional metal oxide catalysts for CO oxidation was measured on the activation energy of the procedure [82]. The activation energy results are very helpful for modeling and planning of catalytic converter. Chemical kinetics are applied on these factors, which can affect the rate of reaction under concern and shows clarification for the certain value of rate and leads to the rate equations, which are very valuable in the reactor design [83]. The catalyst initially

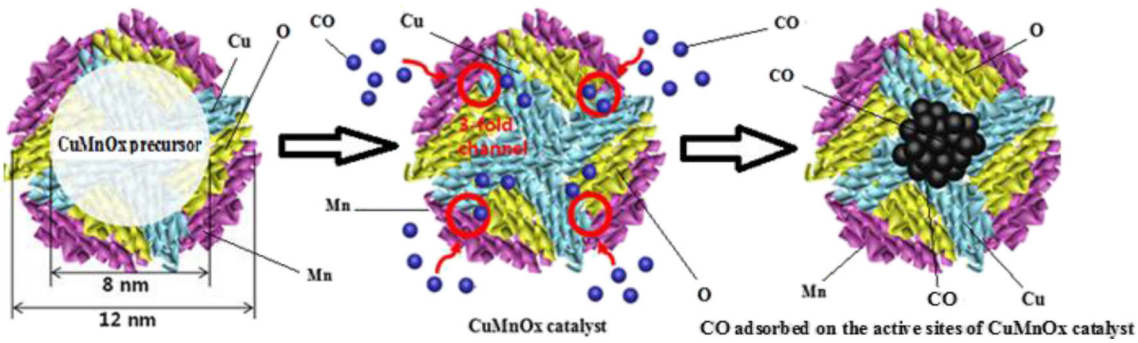

Fig. 11 Physical structure of CuMnOx catalyst and their CO adsorption property

Table 2 The operating parameters and activity measurement of various copper oxide catalysts for CO oxidation

Catalyst	Preparation method	Operating parameters	Remarks	References
CuA	Redox method	The 120 mg catalyst at temp. 35 °C with a gas flow rate 2% CO, 1% O_2 in He. The time taken is 10 h with flow velocity of 20 ccm	CuA (T_{85} = 100 °C at const.)	Xia et al. 1999 [29]
CuO	Self-consistent	The 100 mg catalyst with heating rate 2 °C min^{-1}, in reactive CO–air composition of (2.5–6.0% CO) with total flow velocity of 60 ml/min at atm. pressure	Cu-acetate (T_i = 80 °C, T_{50} = 100 °C, T_{100} = 125 °C) Cu-hydroxide (T_i = 90 °C, T_{50} = 120 °C, T_{100} = 140 °C) Cu-oxalate (T_i = 80 °C, T_{50} = 110 °C, T_{100} = 140 °C) Cu-amino oxalate (T_i = 90 °C, T_{50} = 130 °C, T_{100} = 150 °C) Cu-nitrate (T_i = 130 °C, T_{50} = 160 °C, T_{100} = 170 °C)	Prasad and Singh 2013 [34]
Cu-Cr oxide	Self-propagating high-temperature synthesis	The 0.05% and 0.5% $Pd/Al(NO_3)_3/Al_2O_3$ in reactor with flowing 1% CO in air at a rate of 36,000 h^{-1} in temp. range 100 ± 500 °C. The rate of Ar gas-carrier was 40 ml/min	Al-Cr-Cu-O (T_i = − 60 °C, T_{20} = 500 °C Constant) Cu-Cr-O (T_i = − 100 °C, T_{50} = 250 °C, T_{100} = 350 °C) Ni-Cu-Cr-O (T_i = − 100 °C, T_{50} = 350 °C, T_{70} = 500 °C Constant)	Xanthopoulou and Vekinis 1998 [62]
CuO-TiO_2	Wet impregnation method	The 2 gm catalyst with a reaction gas mixture consists of 5 vol% CO balanced with air. The entire flow of 0.5 l/min and GHSV was 30,000 ml h^{-1} g_{cat}^{-1}	CuO-TiO_2 (T_i = 50 °C, T_{50} = 140 °C, T_{100} = 200 °C)	Dehestaniathar et al. 2015 [72]
CuO Cu_2O	Self-consistent	The 1 gm catalyst with 5 vol% CO/He and pure air at entire flow velocity of 50 cm^3 min^{-1}. The GHSV was 30,000 ml h^{-1} g_{cat}^{-1}	Cu (T_i = 150 °C, T_{50} = 170 °C, T_{100} = 260 °C) CuO (T_i = 80 °C, T_{50} = 140 °C, T_{100} = 165 °C) Cu_2O (T_i = 170 °C, T_{50} = 240 °C, T_{100} = 330 °C)	Nagase et al. 1999 [104]
Cu-Cr catalysts	Impregnation method	The 300 mg catalyst mixed with 100 mg α-alumina gaseous composition of 2% CO, 3% oxygen and balance argon was fed at complete flow velocity of 300 ml/min	CuO (T_i = 125 °C, T_{50} = 165 °C, T_{100} = 195 °C) Cu-Cr/YSZ (T_i = 135 °C, T_{50} = 195 °C, T_{100} = 230 °C)	Huang et al. 1998 [71]
TiO_2(Zr)/CuOx	Impregnation method	The 90 mg catalyst with gases composition of 1 vol.% CO in air and gas flow velocity was 8.65 ml/min and GHSV was 21,000 h^{-1}	Ti/CuOx (T_i = 115 °C, T_{50} = 180 °C, T_{100} = 245 °C) Ti(Zr)/CuOx (T_i = 105 °C, T_{50} = 145 °C, T_{100} = 200 °C) Ti(Si)/CuOx (T_i = 125 °C, T_{50} = 85 °C, T_{100} = 250 °C)	Larsson et al. 1997 [27]
CVD synthesis of Cu_2O	Deposition method	The 15 mg catalyst in a gas composition of 1% CO and 10% O_2 diluted in Ar with a total flow velocity of 15 ml/min and corresponding WHSV was	CVD synthesis of Cu_2O (T_i = 110 °C, T_{50} = 148 °C, T_{100} = 175 °C)	Kasmi et al. 2016 [107]

Table 2 (continued)

Catalyst	Preparation method	Operating parameters	Remarks	References
		60,000 ml g_{cat}^{-1} h^{-1}.		
Cu_XO	Hydrothermal Synthesis	The 30 mg catalyst with heating rate 10 °C/min up to 500 °C. The reaction mixture was consist of 4% CO, 4% O_2 with balanced He, with total flow velocity of 50 ml/min	Cu_2O (T_i = 140 °C, T_{50} = 195 °C, T_{100} = 230 °C) CuO (T_i = 130 °C, T_{50} = 155 °C, T_{100} = 220 °C)	Guo et al. 2015 [108]
Cu_2O	Self-consistent	The 300 mg catalyst with gases compositions of 1.80% CO + 2.95% O_2 in argon and entire flow velocity of 300 ml/min	Cu_2O (T_i = 65 °C, T_{50} = 105 °C, T_{100} = 140 °C)	Huang and Tsai 2003 [109]
CuOx supported Ti/CoOx/FeOx /MnOx	Impregnation method	The 50 mg catalyst in presence of 1.0 vol% CO in air with entire flow velocity of 14.5 l/min and GHSV was 33,500–36,500 h^{-1}	CuOx (T_i = 70 °C, T_{50} = 115 °C, T_{100} = 135 °C) CoOx (T_i = 90 °C, T_{50} = 185 °C, T_{100} = 220 °C) MnOx (T_i = 120 °C, T_{50} = 240 °C, T_{100} = 285 °C) FeOx (T_i = 200 °C, T_{50} = 300 °C Const.) $CuOx/TiO_2$ (T_i = 70 °C, T_{50} = 135 °C, T_{100} = 200 °C)	Larsson et al. 1996 [59]
Cu_2O nanoparticles	Pyrolysis method	The 13 mg catalyst combined with 75 mg of silica gel in presence of 93% N_2, 3% O_2, 4% CO with entire flow velocity of 260 ml/min and GHSV was 200,000 h^{-1}	Cu_2O nanoparticles (T_i = 90 °C, T_{50} = 170 °C, T_{100} = 240 °C)	White et al. 2006 [111]
Cu and Co catalyst	Co-precipitation method/sol-gel method/wet impregnation method	The 100 mg catalyst with 2% CO balanced air at a total flow rate of 100 ml/min	Cu and Co Co-precipitation method (T_i = 25 °C, T_{50} = 80 °C T_{100} = 115 °C) Cu and Co Sol-gel method (T_i = 35 °C, T_{50} = 120 °C, T_{100} = 155 °C) Cu and Co Wet impregnation method (T_i = 55 °C, T_{50} = 110 °C, T_{100} = 150 °C)	Rattan and Kaur 2015 [112]
CuO/TiO_2	Hydrolysis method	The 100 mg catalyst with 1.6% CO, 20.8% O_2, 77.6% N_2 at a space velocity of 30,000 ml/h	$CuTiO_2$ (T_i = 80 °C, T_{50} = 185 °C, T_{100} = 200 °C)	Tang et al. 2016 [76]
CuBTC	Self-consistent	The 100 mg catalyst in gases presence of 1% CO, 0.5% O_2, N_2 as balance. The flow velocity was 30 ml/min and GHSV was 30,000 h^{-1}	CuBTC (T_i = 100 °C, T_{50} = 145 °C, T_{100} = 165 °C)	Wenge et al. 2012 [137]
$CuO-TiO_2$ nanotubes	Impregnation method	The 100 mg catalyst in presence of 1% CO balanced in air at a complete flow velocity of 33.6 ml/min	$CuO-TiO_2$ (T_{100} = 144 °C) $CuO-TiO_2$ nanotubes (T_{100} = 90 °C)	Zhu et al. 2007 [140]
$CuO/CeO_2/ZrO_2$	Impregnation method	The 1.8 gm catalyst with composition: 2 vol% CO, 1.5 vol% O_2, and 96.5 vol% H_2 at SV 12,000 h^{-1}	$CuO/CeO_2/ZrO_2$ (T_i = 35 °C, T_{50} = 80 °C, T_{100} = 145 °C)	Pakharukova et al. 2009 [144]
Ni/Mn-Cu-CrO	Impregnation method	The 100 mg catalyst with gases mixture of 1% CO in air at a	Ni-Cu-CrO	Xanthopoulou and Vekinis 1998 [62]

Table 2 (continued)

Catalyst	Preparation method	Operating parameters	Remarks	References
		flow velocity of 36,000 h^{-1} in a temperature range of 100–500 °C	(T_i = 105 °C, T_{50} = 350 °C, T_{100} = 500 °C) Mn-Cu-CrO (T_i = 100 °C, T_{50} = 320 °C, T_{80} = 500 °C Const.) Cu-CrO (T_i = 100 °C, T_{50} = 240 °C, T_{100} = 350 °C)	
Oil shale ash supported CuO catalyst	Deposition-precipitation method	The 500 mg catalyst in gas composition of 10 vol%, CO balanced air at the time of 30 min. The WHSV was 11,000 ml/h/gm	Oil shale ash (T_i = 215 °C, T_{50} = 280 °C, T_{65} = 350 °C Const.) Oil shale ash supported CuO catalyst (T_i = 120 °C, T_{50} = 135 °C, T_{100} = 190 °C)	CaO et. al. 2015 [66]
$Cu/A1_2O_3$	Impregnation method	The 30 mg catalyst with total flow velocity of (80 cm^3/min) at 4.8% CO/9/8% OJ 85.4% He gas mixture temperature range of 150–400 °C	$Cu/A1_2O_3$ (T_i = 150 °C, T_{50} = 215 °C, T_{100} = 400 °C)	Park and Ledford 1998 [94]
Cu-Cr/γ-alumina catalyst	Co impregnation method	The 100 mg catalyst with 2% CO, 2% oxygen, and balance N_2 at total flow velocity of 500 ml/min. A space velocity of 150,000 h^{-1}	Cu-Cr/γ-alumina catalyst (T_i = 105 °C, T_{50} = 180 °C, T_{100} = 300 °C)	Chien et al. 1995 [97]
CuO supported yttria stabilized zirconia and γ-alumina	Impregnation method	The 100 mg of catalyst with composition of 3% O_2 + 2% CO in Ar with entire flow velocity of 300 ml/min and space velocity was 120,000 h^{-1}	0.5 wt% Pd/γ-alumina (T_i = 145 °C, T_{50} = 170 °C, T_{100} = 200 °C) 0.5 wt% Pt/γ-alumina (T_i = 170 °C, T_{50} = 220 °C, T_{100} = 240 °C) 0.5 wt% Cu/γ-alumina (T_i = 225 °C, T_{50} = 270 °C, T_{100} = 410 °C) 0.4 wt% Cu-YSZ (T_i = 130 °C, T_{50} = 180 °C, T_{100} = 270 °C)	Dow and Huang 1996 [110]
Cu/TiO_2 $Cu-ZnO/Al_2O_3$	Deposition-precipitation method and impregnation method	The 50 mg catalyst in presence of 4.5% CO, 2.23% O_2 balanced He. The total flow velocity was 100 ml/min and space velocity was 10,000 $cm^3/(h.g_{cat})$	Cu/TiO_2 (T_i = 75 °C, T_{50} = 110 °C, T_{100} = 170 °C) $Cu/ZnO/Al_2O_3$ (T_i = 105 °C, T_{50} = 190 °C, T_{100} = 205 °C)	Chen et al. 2012 [113]
$CuO/ZrO_2-Al_2O_3$	Conventional impregnation method	The 500 mg catalyst with gas composition of 2.8 vol% CO and 8.0 vol% O_2 in N_2. The catalyst space velocity was 10,000 h^{-1}	CuO/ZrO_2 (T_i = 50 °C, T_{50} = 115 °C, T_{100} = 130 °C) $CuO/ZrO_2-Al_2O_3$ (T_i = 115 °C, T_{50} = 170 °C, T_{100} = 210 °C) $CuO/γ-Al_2O_3$ (T_i = 220 °C, T_{50} = 250 °C, T_{100} = 300 °C)	Zhou et al. 1997 [143]
CuO/Al_2O_3	Self-consistent	The 100 mg catalyst with CO, O_2, and N_2 with corresponding SV was 50,000 h^{-1}. The total flow rate was 60 ml/min	CuO/Al_2O_3 (T_i = 200 °C, T_{50} = 265 °C, T_{80} = 325 °C Const.)	Snapkauskiene et al. 2011 [92]
Metal organic framework MIL-53(Al) support Cu	Solvothermal method	The 100 mg catalyst with feed gas mixture of 1.45% CO, 1.5% O_2, and 55% H_2 with balance gas N_2. The flow rate was 50 ml/min in temperature	MIL-53(Al) support Cu (T_i = 120 °C, T_{50} = 230 °C, T_{100} = 245 °C)	Tan et al. 2015 [15]

Table 2 (continued)

Catalyst	Preparation method	Operating parameters	Remarks	References
		range 50 °C for 2 h		
CuO/Al_2O_3	Impregnation method	The 150 mg catalyst with complete flow velocity of 80 ml/min, the gases consists of 2.5% CO and 1.45% O_2 in N_2.	CuO/Al_2O_3 (T_i = 150 °C, T_{50} = 175 °C, T_{100} = 230 °C)	Luo et al. 2005 [63]

oxidized CO before it is oxidized by air and this is an investigation by the Mars-van Krevelen-type mechanism, which has certainly found on the support. A Langmuir-Hinshelwood-type mechanism between adsorbed oxygen and CO has been applied, and it is not clear if operates completely or there is a combination of both.

The oxidation of CO by the Mars-van Krevelen mechanism would represents the correlation between Co_3O_4 catalyst activity and reducibility [79]. The conversion of CO over cobalt oxide catalyst could be discussed very well by the Langmuir-Hinshelwood model, in which molecularly chemisorbed CO reacts with dissociative adsorbed oxygen in the first-order reaction. Figure 19a represents the Langmuir-Hinshelwood mechanism for CO conversion on the Co_3O_4 metal surface. In the initial step of reaction, CO and O_2 adsorb into the catalyst surface. Then after, the adsorbed O_2 molecules separate into single O atoms [80]. The CO molecules and O atoms initiate to disperse on the exterior surface, and once a CO molecule and O atom combines each other, they recombine and produced CO_2. In the next step, CO_2 desorbs into the gas phase. The Eley-Rideal mechanism is shown in Fig. 19b, where the reactant molecules adsorbs initially into the Co_3O_4 catalyst surface and reaction was done when other reactant molecule combines it from the gas phase [84].

Finally, the Mars-van Krevelen mechanism is shown in Fig. 19c. Here the gas-phase molecules contact with the oxidized surface. In this procedure, CO contacts with the uppermost oxygen lattices and free the surface by producing CO_2 [85]. In Fig. 19a and Fig. 19b, the blue spheres represent the Co_3O_4 atoms and Fig. 19c represents metal oxide film developed on the summit of substrate (gray atoms). The green spheres represent metal atoms. The red and black spheres in Fig. 19a, b, and c represent oxygen and carbon atoms, respectively. Thin oxide films developed on metal surfaces can be used for mechanism analysis. These thin oxide films should be thick enough to imitate the metal oxide as shown in Fig. 20 of

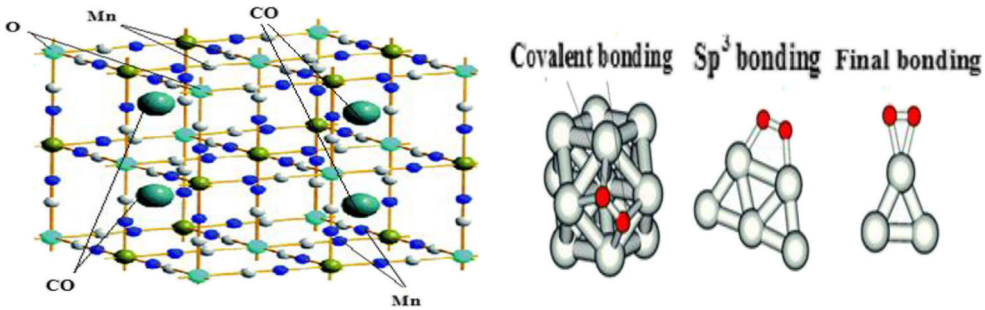

Fig. 12 Chemisorptions of CO over manganese oxide catalysts

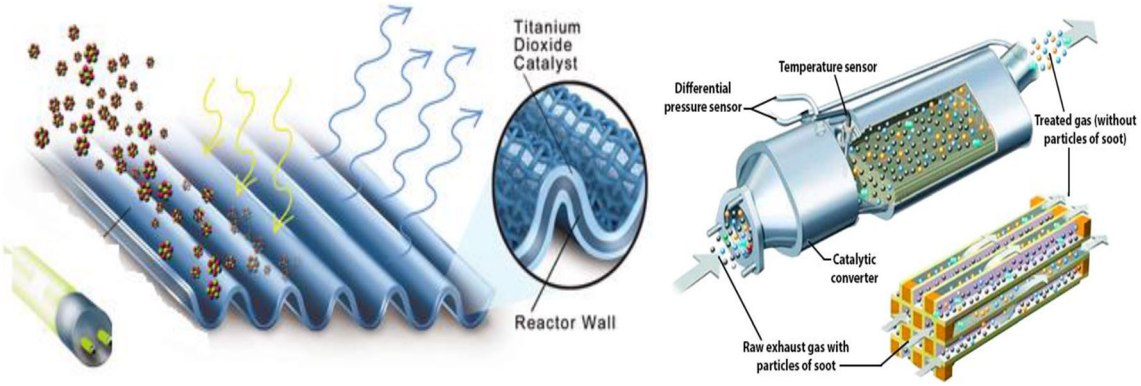

Fig. 13 Catalytic activity of TiO_2 catalysts for CO oxidation

Table 3 The operating parameters and activity measurement of various iron oxide catalysts for CO oxidation

Catalyst	Preparation method	Operating parameters	Remarks	References
Nanosized Fe_2O_3	Co-precipitation method	The catalyst weight 0.3, 1, 2, and 3 g in presence of 24% CO, 38% O_2, 38% N_2 with temp. range 200–500 °C	Nanosized Fe_2O_3 (Ti = 200 °C, T_{50} = 320 °C, T_{100} = 500 °C)	Halim et al. 2006 [102]
Nanosized Fe_xO_y	Precipitation method	The 50 mg catalyst with reactant gases (1% CO and 0.603 vol% H_2O in air) and temp. increased from ambient to 160 °C at the rate of 2 °C/min	Nanosized Fe_xO_y (Ti = 24 °C, T_{50} = 83 °C, T_{100} = 210 °C)	Lin et al. 2005 [36]
CuO-Fe_2O_3	Surfactant-assisted method	The 200 mg catalyst in 10 vol% CO balanced with air at a total flow velocity of 36.6 ml/min and WHSV was 11,000 ml/gh	Fe_2O_3 (T_i = 140 °C, T_{50} = 220 °C, T_{100} = 280 °C) CuO-Fe_2O_3 (T_i = 40 °C, T_{50} = 80 °C, T_{100} = 105 °C)	Cao et al. 2008 [85]
Fe-Cu mixed metal oxide nanopowder	Sol-gel method	The 100 mg catalyst with reaction gases presence of 25% O_2 and 2.5% CO, balanced inert gases	Pure Fe_2O_3 (T_i = 100 °C, T_{50} = 200 °C, T_{100} = 280 °C) Fe-Cu (T_i = 40 °C, T_{50} = 115 °C, T_{100} = 150 °C)	Amini and Rezaei 2015 [88]
α-Fe_2O_3 nanoparticles	Hydrothermal method	The 100 mg catalyst with gases compositions 3.45% CO, 6.76% O_2, and balanced N_2 at 300 ml/min at a temp. range of 150 to 400 °C	α-Fe_2O_3 nanoparticles (T_i = 150 °C, T_{50} = 240 °C, T_{100} = 335 °C)	Hu et al. 2007 [93]
Nano FeOx	Self-consistent	The 40 mg catalyst with a gas mixture of 3.44 vol% CO and 20.6 vol% O_2 balanced He at a total flow velocity of 55 cm^3/min	Nano FeOx (T_i = 160 °C, T_{50} = 320 °C, T_{100} = 500 °C)	Kwon et al. 2007 [38]
Fe_2O_3 nanoparticles	Self-consistent	The 50 mg catalyst with inlet gas composition of 3.44% CO and 20.6% O_2 at 1000 ml/min. The heating rate 12 °C/min	Fe_2O_3 nanoparticles (T_i = 160 °C, T_{50} = 260 °C, T_{100} = 320 °C)	Li et al. 2003 [68]
Nanosized Fe catalyst	Wet impregnation method	The 200 mg catalyst at total flow velocity of 100 ml/min and gases composition of 24% CO, 38% O_2, and 38% N_2.	Nanosized Fe catalyst (T_i = 250 °C, T_{50} = 370 °C, T_{100} = 480 °C)	Khedr et al. 2006 [102]
Fe catalyst	Self-consistent	The 100 mg catalyst with total flow rate of 35.5 ml/min and reaction gas consisted of 37.5% H_2, 2.0% CO, 25.0% H_2O, N_2 (balance)	Fe catalyst (T_i = 70 °C, T_{50} = 135 °C, T_{100} = 240 °C)	Loaiza-Gil et al. 1999 [69]
Fe_2O_3	Polyvinyl alcohol method	The 29 mg catalyst with 1 vol% CO, 5 vol% H_2, 95 vol% N_2 was added at a entire flow velocity of 100 ml/min (STP) and SV was 10,000 h^{-1}	Fe_2O_3 (T_i = 300 °C, T_{50} = 385 °C, T_{100} = 425 °C)	Wagloehner et al. 2008 [106]
Fe_2O_3-NiO	Thermal analysis method	The 100 mg catalyst with 1.5 vol% CO, 2 vol% O_2 balanced with N_2 at flow velocity of 100 ml/min	Fe_2O_3-NiO (T_i = 360 °C, T_{50} = 545 °C, T_{100} = 830 °C)	Li et al. 2014 [114]
Ir/FeOx	Citric acid sol-gel and precipitation method	The 200 mg catalyst with 1% CO in air at a WHSV of 15,000 ml/(g.h)	FeOx (T_i = 170 °C, T_{50} = 245 °C, T_{100} = 290 °C) Ir/FeOx (T_i = − 40 °C, T_{50} = 0 °C, T_{100} = 40 °C)	Zhang et al. 2015 [115]
CuO/Fe_2O_3	Co-precipitation method	The 100 mg catalyst with flow velocity of 30 ml/min and reaction gases consisting of 2.5% CO, 10% O_2, 87.5% N_2	CuO/Fe_2O_3 (Ti = 40 °C, T_{50} = 80 °C, T_{100} = 100 °C)	Cheng et al. 2007 [138]
Fe-MCM41	Sol-gel method	The 100 mg catalyst with total flow velocity of 70 ml/min,	Fe-MCM-41	Szegedi et al. 2004 [139]

Table 3 (continued)

Catalyst	Preparation method	Operating parameters	Remarks	References
		P_{CO} = 16 Torr, P_{O2} = 16 Torr, heating rate 10 K.min^{-1}	(Ti = 10 °C, T_{50} = 40 °C, T_{100} = 100 °C)	
$NiFe_2O_4$ $La_{0.8}Pb_{0.2}Fe_{0.8}Co_{0.2}O_3$	Wet chemical Pechini route	The 100 mg catalyst in presence of 2 ppm CO, 5 ppm N_2 balanced air at temp. 100 °C for 2 h	$NiFe_2O_4$ (T_i = 125 °C, T_{50} = 210 °C, T_{100} = 280 °C) $La_{0.8}Pb_{0.2}Fe_{0.8}Co_{0.2}O_3$ (Ti = 85 °C, T_{50} = 130 °C, T_{100} = 175 °C)	Maity et al. 2016 [142]
Fe-Mn/K/Al_2O_3	Co-precipitation method	The 100 mg catalyst with total flow velocity of 30 ml/min and GHSV was 2000–7200 h^{-1}. The H_2/CO was 1.6	Fe-Mn/K/Al_2O_3 (T_i = 210 °C, T_{50} = 300 °C Const.)	Fazlollah et al. 2013 [91]

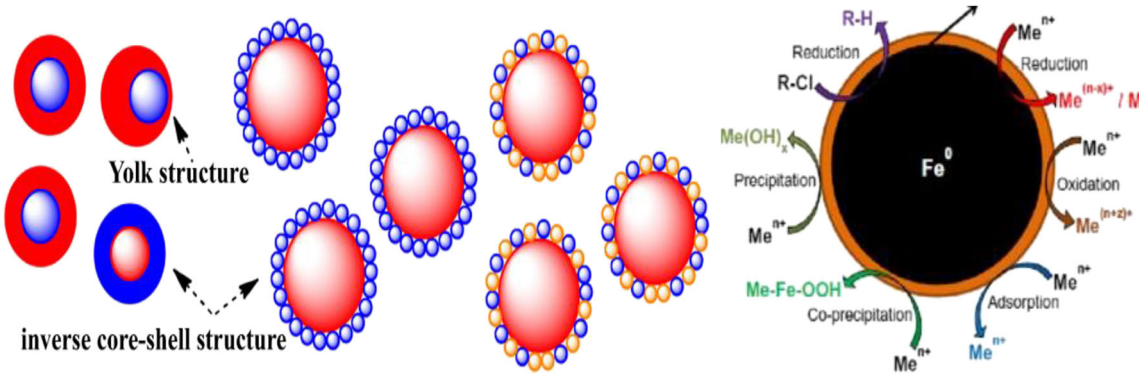

Fig. 14 Chemisorptions of CO over iron nanoparticles

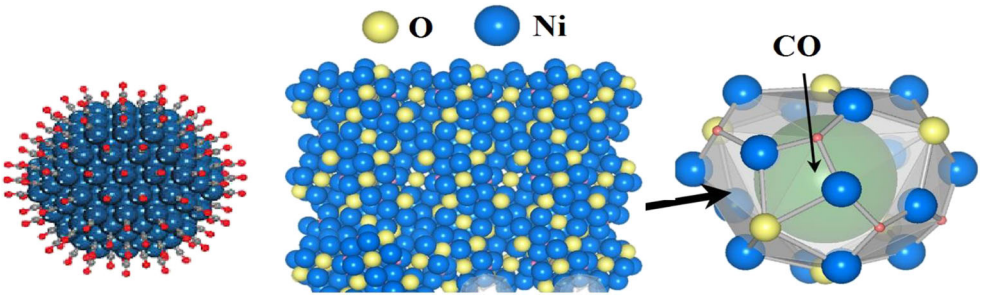

Fig. 15 Chemical bonding of carbon monoxide with NiO catalyst

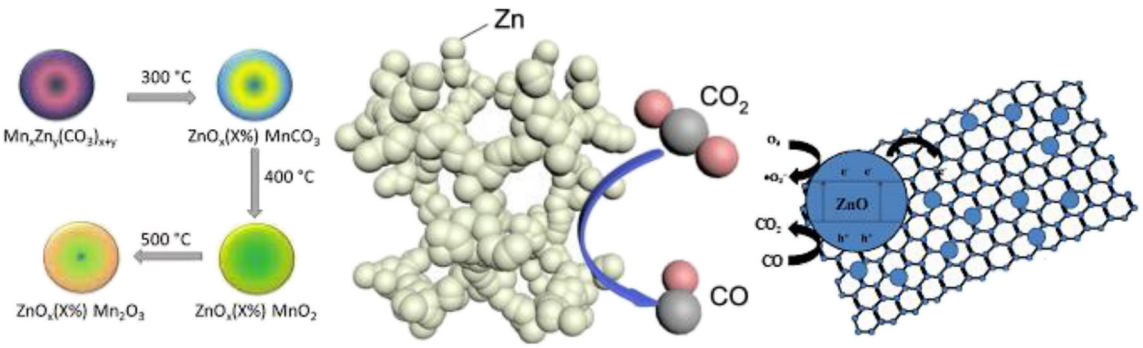

Fig. 16 Structural bonding of zinc oxide with carbon monoxide

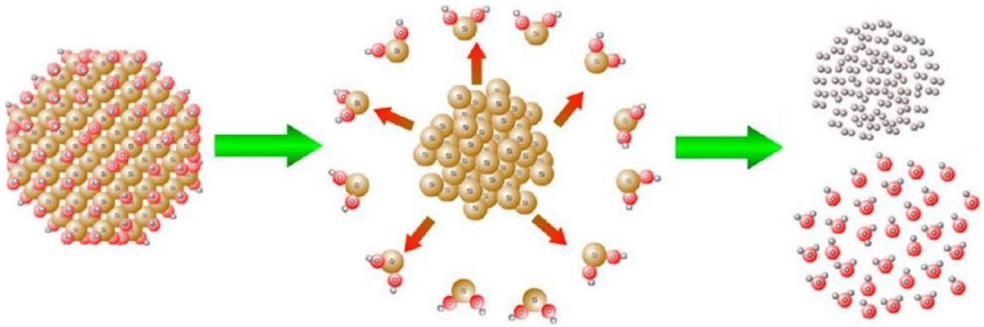

Fig. 17 Structural arrangement of chromium oxide catalyst for CO chemisorptions

the real oxide, but thin and thereby conductive adequate to allocate electron-based techniques to be applied.

Such thin cobalt oxide films are frequently formed by depositing and oxidizing a metal on an individual crystal surface. A catalytic reaction on the surface of catalyst and gas surface interface includes the observation of gas adsorption, dissociation, diffusion, and desorption. Gas adsorption as shown in Fig. 21 can be divided into dual categories depending on the strength of adsorbate-surface interface: (i) if adsorbate CO is combine to the catalyst surface by lose Van der Waals bonds, it represents to the adsorption process as physic-sorption and (ii) if actual chemical bonds are produced in the adsorbate CO on catalyst surface, it represents to the adsorption process as chemisorptions [86]. In the physic-sorption process, the adsorbates are captured at certain space from catalyst surface and no valence electrons are replaced with the surface. In

Table 4 The operating parameters and activity measurement of various manganese oxide catalysts for CO oxidation

Catalyst	Preparation method	Operating parameters	Remarks	References
Cryptomelane MnOx	Milling method	The 100 mg catalyst in presence of 2% CO, 1% O_2, and remaining N_2. The total flow velocity was 100 ml/min, GHSV was 3000 h^{-1}	Cryptomelane MnOx (T_i = 80 °C, T_{50} = 120 °C, T_{75} = 160 °C Const.)	Hernandez et al. 2010 [65]
Fe-Mn/ZSM-5	Incipient wetness method	The 500 mg catalyst at pressure 1 bar GHSV was 1000 h^{-1}. The H_2/CO is 2 at temperature 250 °C	Fe-Mn/ZSM-5 (T_i = 140 °C, T_{50} = 220 °C, T_{100} = 310 °C)	Feyzi et al. 2015 [83]
Mn_3O_4 nanorods	Dispersion-precipitation method	The 0.1 gm catalyst with CO concentration 10,000 ppmv balanced with air. The total flow velocity was 50 ml/min and GHSV was 30,000 h^{-1}	Mn_3O_4 nanorods (T_i = 35 °C, T_{50} = 90 °C, T_{100} = 115 °C)	Li et al. 2013 [86]
MnOx	Incipient wetness impregnation method	The 100 mg catalyst in 10,000 ppm CO balanced air. The total gases flow rate was 50 ml/min and GHSV was 32,500 h^{-1} at temp. 140 °C	MnOx (T_i = 50 °C, T_{50} = 90 °C, T_{100} = 130 °C) HNO_3-MnOx (T_i = 80 °C, T_{50} = 170 °C, T_{100} = 180 °C)	Li et al. 2014 [141]
Mn-acetate Mn-Nitrate	Precipitation method	The 100 mg catalyst in 1.5% CO in air at entirety flow velocity was 60 ml/min and GHSV at temp. 125 °C	Mn-acetate (T_i = 25 °C, T_{50} = 70 °C, T_{100} = 130 °C) Mn-nitrate (T_i = 25 °C, T_{50} = 80 °C, T_{100} = 160 °C)	Dey et al. 2018 [10]
MnOx	Incipient wetness impregnation method	The 50 mg catalyst in 1.5% CO balanced air. The total flow rate was 60 ml/min and GHSV was 35,000 h^{-1} at temp. 120 °C	MnOx (T_i = 25 °C, T_{50} = 65 °C, T_{100} = 125 °C)	Ye et al. 2018 [153]
MnOx	Precipitation method	The 100 mg catalyst in 1.5% CO in air with entirely flow rate was 60 ml/min and GHSV at temp. 125 °C	MnOx (T_i = 20 °C, T_{50} = 70 °C, T_{100} = 120 °C)	Dey et al. 2018 [12]
Mo/γ-Al_2O_3	Incipient wetness impregnation method	The 50 mg catalyst (15 wt%) with 1.65% CO, 2.5% O_2, and 2.75% balanced N_2. The GHSV was 42,000 $cm^3/g_{cat}h$ and complete flow velocity was 60 ml/min	γ-Al_2O_3 (T_i = 40 °C, T_{50} = 145 °C, T_{100} = 165 °C) Mo/γ-Al_2O_3 (T_i = 40 °C, T_{50} = 145 °C, T_{100} = 165 °C)	Liu et al. 2015 [13]

Table 5 The operating parameters and activity measurement of various nickel oxide catalysts for CO oxidation

Catalyst	Preparation Method	Operating Parameters	Remarks	References
Ni-based alloys	Melt spinning technique	The 20 mg catalyst with a gas composition of 98% H_2, 2% CO, and 4% O_2 at temp. 155 °C, atm. pressure	Ni-based alloy (T_i = 157 °C, T_{50} = 250 °C, T_{100} = 327 °C)	Stancheva et al. 1996 [58]
Ni/TiO_2	Impregnation method	The 500 mg catalyst with entire flow velocity of 30 ml/min. The feed gases compositions of 1.75% CO, 1.75% O_2, 25% H_2 balanced N_2. The GHSV was 20,000 h^{-1}	Ni/TiO_2 (T_i = 15 °C, T_{50} = 30 °C, T_{100} = 50 °C)	Wu et al. 2005 [90]
$NiFe_2O_4$	Wet chemical Pechini route	The 100 mg catalyst in presence of 2 ppm CO, 5 ppm N_2 remaining air at temp. 100 °C for 2 h	$NiFe_2O_4$ (T_i = 125 °C, T_{50} = 210 °C, T_{100} = 280 °C)	Maity et al. 2016 [142]
Ni-Cu-CrO	Impregnation method	The 100 mg catalyst in presence of 1% CO in air at a total flow velocity 36,000 h^{-1} in a temperature range of 100–500 °C	Ni-Cu-CrO (T_i = 105 °C, T_{50} = 350 °C, T_{100} = 500 °C)	Xanthopoulou and Vekinis 1998 [62]
NiOx	Thermal-reforming method	The 100 mg catalyst at temp. 25 °C with a gases flow rate 3.5% CO, 1.5% O_2 in He. The complete flow velocity of 20 ml/min to space velocity was 4000 ml $gcat^{-1}$ h^{-1}	NiOx (T_i = 75 °C, T_{50} = 110 °C, T_{100} = 145 °C)	Park et al. 2019 [152]
Ni-Co-O	Liquid precipitation method	The 50 mg catalyst with 1.65% CO, 20.8% O_2, and 77.6% N_2. The space velocity was 30,000 $ml.h^{-1}$ gca^{t-1}	NiOx (T_i = 55 °C, T_{50} = 150 °C, T_{100} = 215 °C) $Ni_{0.2}Co_{0.8}$ (T_i = 50 °C, T_{50} = 80 °C, T_{100} = 120 °C)	Yi et al. 2018 [153]
NiOx	Precipitation method	The 100 mg catalyst consisting of 1.5 vol% CO balanced with air. The complete flow velocity was 35.5 ml/min and WHSV was 12,000 ml/h/g	NiOx (T_i = 35 °C, T_{50} = 110 °C, T_{100} = 165 °C)	Parravano 1953 [154]
Ni-Al_2O_3 catalysts	Deposition-precipitation method	The 100 mg catalyst with a reactant gases composition of 1.5 vol% CO in air. The entire flow velocity was 45 ml/min and GHSV was 320,000 ml h^{-1} g_{cat}^{-1}	Ni-Al_2O_3 (T_i = 40 °C, T_{50} = 70 °C, T_{100} = 145 °C)	Jiajian et al. 2013 [159]
NiO supported Al_2O_3	Deposition process	The 2 gm catalyst with 1% CO in air with complete flow velocity was 10 ml/min and space velocity was 60,000 ml/hg_{cat}	NiO supported Al_2O_3 (T_i = 200 °C, T_{50} = 375 °C, T_{100} = 600 °C)	Han et al. 2016 [136]

comparison, the replacement of valence electrons has done among the catalyst surface and CO adsorbate for the chemisorptions process [87].

$$O_2 + 2* \rightarrow 2O_{ads} \quad (1)$$

$$CO + * \rightarrow CO_{ads} \quad (2)$$

$$CO_{ads} + O_{ads} \rightarrow CO_2 + 2* \quad (3)$$

Depending on the nature of surface, the molecular chemisorptions can be done, or the molecules instinctively separate upon the adsorption. The distinction of oxygen molecules was done by the reaction between adsorbed oxygen atom and CO to CO_2 is individual one of the accepted mechanisms for CO conversion. In this situation, the reaction rate was limited by the dissociation of O_2. The molecular chemisorptions of CO can be done at the higher temperatures, which ensure that the appearance of reactive oxygen forms [88]. The O^- ions are highly reactive and performances of superoxide are also increase, although much poorer as compared to O^-. In oxygen species, the CO molecules from the gas phase can be oxidized. The concentration of adsorbed oxygen produced does not include to the concentration of transition metals, but its presence represents the development of these products [89, 90], where * represents a free site on the metal surface. The CO_2 produced as shown in Fig. 22 is simply adsorbed and does not influence the rate significantly, since it is rapidly desorbed into the gas phase. No surface carbonate species are produced as intermediate in this reaction.

The reaction rate will be proportional to the surface exposure of O_{ads} and CO_{ads}. The oxidation occurs in two steps. First, the CO is oxidized by exterior lattice oxygen in the metal oxide. An oxygen vacancy was produced, decreasing the nearest metal ions to a poorer oxidation state. In the second step, the exterior surface metal atoms are oxidized by the gas-phase oxygen [91]. The differences of activity and binding energy of transition metal catalysts were noted as a function of capacity factor for the series of catalysts.

Table 6 The operating parameters and activity measurement of various titanium oxide catalysts for CO oxidation

Catalyst	Preparation method	Operating parameters	Remarks	References
Pt/TiO_2	Deposition-precipitation method	The 100 mg catalyst in 12,000 ppm CO balanced air. The total flow velocity was 50 ml/min and GHSV was 35,000 h^{-1} at temperature 140 °C	TiO_2 (T_i = 35 °C, T_{50} = 90 °C, T_{100} = 115 °C)	Bonanni et al. 2012 [133]
$CuO-TiO_2$	Wet impregnation method	The 2 gm catalyst with a reaction gases compositions of 5 vol% CO balanced with air. The total gases flow was 0.5 l/min and GHSV was 30,000 ml h^{-1} g_{cat}^{-1}.	$CuO-TiO_2$ (T_i = 50 °C, T_{50} = 140 °C, T_{100} = 200 °C)	Dehestaniathar et al. 2015 [72]
TiCrOx	Sol-gel method	The 20 mg catalyst mixed with 100 mg SiO_2 at a feed rate ($C_3H_8/CO/CO_2/O_2/N_2$ = 2.23/10.56/15.48/111.56/62.46 vol%) in air had a total gases flow of 50 ml/min	TiCrOx (T_i = 100 °C, T_{50} = 140 °C, T_{100} = 225 °C)	Swislocki et al. 2014 [37]
Ni/TiO_2	Impregnation method	The 500 mg catalyst with entire flow velocity 30 ml/min. The feed gases mixture of 1.65% CO, 1.58% O_2, 23% H_2 balanced N_2. The GHSV was 20,000 h^{-1}	Ni/TiO_2 (T_i = 15 °C, T_{50} = 30 °C, T_{100} = 50 °C)	Wu et al. 2005 [90]
TiO_2(Zr)/CuOx	Impregnation method	The 90 mg catalyst with gases mixture of 1 vol.% CO in air and gas flow velocity was 8.65 ml/min and GHSV was 21,000/h	Ti/CuOx (T_i = 115 °C, T_{50} = 180 °C, T_{100} = 245 °C) Ti(Zr)/CuOx (T_i = 105 °C, T_{50} = 145 °C, T_{100} = 200 °C) Ti(Si)/CuOx (T_i = 125 °C, T_{50} = 85 °C, T_{100} = 250 °C)	Larsson et al. 1997 [27]
Pt_1/VC-TiC(001)	Impregnation method	The 100 mg catalyst in 12,000 ppm CO balanced air. The entire flow velocity was 60 ml/min and GHSV was 30,000 h^{-1} at temp. 140 °C	Pt_1/VC-TiC(001) (T_i = 65 °C, T_{50} = 96 °**C**, T_{100} = 135 °C)	Wang et al. 2018 [134]
Cu/TiO_2	Deposition-precipitation and impregnation method	The 50 mg catalyst with 4.5% CO, 2.23% O_2 remaining He. The total flow rate was 100 ml/min and SV was 10,000 $cm^3/(h.g_{cat})$	Cu/TiO_2 (T_i = 75 °C, T_{50} = 110 °C, T_{100} = 170 °C)	Chen et al. 2012 [113]
$CuO-TiO_2$ nanotubes	Impregnation method	The 100 mg catalyst in reaction mixture of 1% CO balanced air at a complete flow velocity of 33.6 ml/min	$CuO-TiO_2$ (T_{100} = 144 °C) $CuO-TiO_2$ nanotubes (T_{100} = 90 °C)	Zhu et al. 2007 [140]
CoOx- TiO_2	Incipient wetness impregnation method	The 0.05 gm of catalyst and gases consisting of 1% CO in air with total flow velocity of 100 ml/min and WHSV = 120,000 ml/h.g	Au/3% CoOx-TiO_2 (T_i = 25 °C, T_{50} = 50 °C, T_{100} = 80 °C)	Lee and Chen 2013 [151]
$Au/Al_2O_3-TiO_2$	Deposition-precipitation method	The 30 mg catalysts in presence of reaction mixtures 1%vol CO, 9%vol He, 17.8% vol O_2, and 72.2% vol N_2 with total flow velocity of 100 cm^3/min	$Au/Al_2O_3-TiO_2$ (T_i = 45 °C, T_{50} = 70 °C, T_{100} = 115 °C)	Rajska et al. 2016 [150]

CO is react with chemisorbed oxygen as shown in the Fig. 23 either adding on it from the gas phase or produced an adsorbed state subsequently to the adsorbed oxygen or on the peak of adsorbed oxygen. In reaction conditions, the rate was proportional to the O_2 pressure and independent of CO pressure. The rate of CO oxidation was determined by following either the rate of production of CO_2 or when the CO was captured and rate of disappearance of CO [92]. The reaction rate was found to be reduced when CO was introduced into the gas phase during the oxidation. The first-order reaction in CO can be done due to the reaction from as lower chemisorbed layer or although the reaction from the gas phase

Table 7 The operating parameters and activity measurement of various zinc oxide catalysts for CO oxidation

Catalyst	Preparation method	Operating parameters	Remarks	References
Zn-Cu-Ti	Co-precipitation method	The 100 mg catalyst with 1.5% CO in air. The entire flow velocity was 100 ml/min	Zn-Cu-Ti (T_i = 200 °C, T_{50} = 230 °C, T_{100} = 270 °C)	Saber and Zaki 2014 [155]
Cu-Zn	Co-precipitation method	The 100 mg catalyst with 2% CO balanced air with complete flow rate of 100 ml/min	Cu-Zn (T_i = 85 °C, T_{50} = 157 °C, T_{100} = 225 °C)	Chafidz et al. 2018 [157]
Cu-Zn-CeO_2	Polyol method	The 300 mg catalyst with of 1.5% CO in the air with complete flow velocity was 60 ml/min	Cu-Zn-CeO_2 (T_i = 105 °C, T_{50} = 185 °C, T_{100} = 240 °C)	Allam et al. 2019 [158]
ZnO·CrO_3	Precipitation method	The 100 mg catalyst with 1.0 vol% CO in air with entire feed rate was 14.5 l/min and GHSV was 33,5000 h^{-1}	$ZnCr_2O_4$ (T_i = 85 °C, T_{50} = 145 °C, T_{100} = 210 °C)	Gac et al. 2016 [156]
Cu-ZnO/Al_2O_3	Impregnation method	The 50 mg catalyst with 4.5% CO, 2.23% O_2 balanced He. The complete flow rate was 100 ml/min and space velocity was 10,000 $cm^3/(h.g_{cat})$	Cu/ZnO/Al_2O_3 (T_i = 105 °C, T_{50} = 190 °C, T_{100} = 205 °C)	Chen et al. 2012 [113]

[93]. The amount of CO_2 molecules chemisorbed corresponded to the amount of oxygen atoms pre-adsorbed on the catalyst surfaces. With the equal concentration of oxygen atoms in the gas phase over the surface, therefore, heterogeneous exchange reaction was taking places. The mechanisms of CO oxidation on the surfaces of catalysts are a top tactic in nature, thus responsible for the loss and uptake of bulk oxygen for the production and disappearance of vacancies as explained in these systems as attractive oxidation catalysts [94]. The incompatible oxygen stoichiometry of TMO structure is responsible for extraordinary performance of these materials [95]. For stable oxides, the rate-determining step will be the reaction between CO_{ads} and O_{ads}, while for a TMO that has an inferior M-O bond energy, the rate-determining step will be adsorption or dissociation of molecular oxygen on the metal surface. Accordingly, the CO oxidation processes to occur with high reaction rates if CO, adsorbed on the metal particle, interacts with oxygen adsorbed on an extremely reducible metal oxide support, with following dissociation at the metal–support boundary [96, 97]. The theoretical calculations suppose that the CO was oxidized by reaction with atomically adsorbed oxygen in a Langmuir-Hinshelwood mechanism. The Langmuir-Hinshelwood model has been explained in the CO oxidation mechanism taking place on transitional metal oxide catalysts [98]. In the Langmuir-Hinshelwood model, the CO conversion occurs on the exterior surface in the following steps are involved:

$$CO(g) \rightarrow CO_{ads} \quad (4)$$

$$O_2(g) \rightarrow 2O_{ads} \quad (5)$$

$$CO_{ads} + O_{ads} \rightarrow CO_2(g) \quad (6)$$

In this analysis, the function of substrate (such as Fe_2O_3, TiO_2, NiO, Co_3O_4) is not constant with the small supported particles as represented in Fig. 24, but smooth to advance the adsorption and activation of oxygen. For non-reducible supports, such as SiO_2 and Al_2O_3, the catalytic performances were much more strongly dependent on the transitional metal diffusion; in fact, the oxygen adsorption has done only the metal sites [99, 100].

The CO conversion over unsupported transitional metal oxides takings according to a Langmuir-Hinshelwood mechanism was noted, in which the determining steps occur in the adsorbed phase. Both reactants are adsorbed [101]. The boundary of metal oxide and support is of particular interest since transition metal can act as a strong promoter to TMO for CO oxidation reaction. The goal of this work is to improve our understanding of the chemical process taking place on the transition metal catalysts [102].

6 Deactivation of transition metal catalysts

The performances and selectivity of transition metal catalysts in catalytic converter are essential for CO conversion reaction. The catalyst deactivation and failure over in catalytic performances create problem in the practice of catalytic process. The catalyst deactivation can be divided into six different types: (i) poisoning, (ii) thermal degradation, (iii) fouling, (iv) vapor compound formation, solid-solid and/or vapor-solid reactions, and (vi) crushing/abrasion [103]. The major reason of catalyst deactivation was divided into three parts: chemically, mechanically and thermally. The lead, sulfur poisoning, carbon production, and sintering are the major cause of catalyst deactivation. The dispersion of active phase rapidly decreases, which is one of the major reasons of catalyst deactivation as shown in Fig. 25 and Fig. 26.

The transition metal catalyst was easily deactivated by a trace amount of moisture present in the catalyst [104–107]. The substitutions of materials in transition metal catalysts should not affect their performance in reforming reaction; at the same time, these changes in the structure should keep their resistance to carbon deposition as well as to sulfur poisoning.

Table 8 The operating parameters and activity measurement of various chromium oxide catalysts for CO oxidation

Catalyst	Preparation method	Operating parameters	Remarks	References
TiCrOx	Sol-gel method	The 20 mg catalyst mixed with 100 mg SiO_2 at a feed rate (C_3H_8/CO/CO_2/O_2/N_2 = 2.5/10.65/15.76/10/62.5 vol%) in air and entire flow velocity was 55 ml/min	TiCrOx (T_i = 100 °C, T_{50} = 140 °C, T_{100} = 225 °C)	Swislocki et al. 2014 [37]
Cu-Cr catalysts	Impregnation method	The 300 mg catalyst mixed with 100 mg α-alumina in gaseous composition of 2% CO, 3% O_2, and balance Ar with total flow velocity of 300 ml/min	Cu-Cr/YSZ (T_i = 135 °C, T_{50} = 195 °C, T_{100} = 230 °C)	Huang et al. 1998 [71]
Cu-Mn-Cr	Impregnation method	The 100 mg catalyst in presence of 2 ppm CO, 5 ppm N_2 balanced air at temp. 100 °C for 2 h	Cu-Mn-Cr (T_i = 35 °C, T_{50} = 105 °C, T_{100} = 180 °C)	Ivanov et al. 2015 [126]
$CuCr_2O_4$	Co impregnation method	The 100 mg catalyst with 1.5 vol% CO in air with total feed rate of 16.5 l/min and GHSV of 35,000 h^{-1}	$CuCr_2O_4$ (T_i = 102 °C, T_{50} = 210 °C, T_{100} = 320 °C)	Prasad and Singh 2012 [149]
Cr-oxide/MCM-41	Incipient wetness method	The 50 mg catalyst with 1 vol% CO, 1 vol% O_2 in air with entire flow velocity of 30 cm^3/min	Cr-oxide/MCM-41 (T_i = 75 °C, T_{50} = 165 °C, T_{100} = 270 °C)	Michorczyk et al. 2008 [128]
Cr_2O_3/Al_2O_3	Incipient wetness impregnation method	The 100 mg catalyst with complete flow velocity of 60 ml/min and (GHSV) of 6200 h^{-1}	Cr_2O_3/Al_2O_3 (T_i = 120 °C, T_{50} = 235 °C, T_{100} = 340 °C)	Cherian et al. 2002 [130]
Cr_2O_3/ZrO_2 Cr_2O_3/γ-Al_2O_3 Cr_2O_3/SBA-15	Impregnation method	The 200 mg catalyst with entire flow velocity of 20 ml/min and reaction gas mixture consists of 2.5% CO, 2.5% O_2, and balanced N_2	Cr_2O_3/ZrO_2 (T_i = 70 °C, T_{50} = 145 °C, T_{100} = 225 °C) Cr_2O_3/γ-Al_2O_3 (T_i = 105 °C, T_{50} = 185 °C, T_{100} = 270 °C) Cr_2O_3/SBA-15 (T_i = 145 °C, T_{50} = 215 °C, T_{100} = 315 °C)	Zhang et al. 2002 [129]
Cu-Cr/γ-alumina catalyst	Co impregnation method	The 100 mg catalyst in presence of 2% CO, 2% oxygen, and balance N_2 at total flow rate of 500 ml/min. A SV of 150,000 h^{-1}	Cu-Cr/γ-alumina catalyst (T_i = 105 °C, T_{50} = 180 °C, T_{100} = 300 °C)	Chien et al. 1995 [97]
Co-Cr-Al-O	Self-propagating high-temperature synthesis method	The 100 mg catalyst with 1% CO in air at a space velocity of 2000 h^{-1}	Co-Cr-Al-O (T_i = 80 °C, T_{50} = 155 °C, T_{100} = 210 °C)	Tyurkin et al. 1997 [100]
Cr_2O_3/Al_2O_3	Nanocasting method	The 200 mg catalyst in presence of 2.5 vol% CO and 1.5 vol% O_2 in N_2. The complete flow velocity was 30 cm^3/min	Cr_2O_3/Al_2O_3 (T_i = 52 °C, T_{50} = 140 °C, T_{100} = 210 °C)	Wegrzyniak et al. 2007 [127]

The stability of transition metal catalyst could be recognized to the more movement of oxygen on the interface of mixed oxides [108–110]. To decrease the deactivation of transition metal catalyst, a certain amount of support materials like SiO_2, TiO_2, and Al_2O_3 was added into the transition metal catalyst and also improves the catalyst [111–113]. The deactivation trend of transition metal catalyst for the mixed stream oxidation suggests that the operating costs for this catalyst would rise rapidly with time on stream [76]. Chemical poisoning, coke formation, and dispersion of active phases are one of the main reasons for catalytic deactivation [114, 115].

The deactivation of transition metal catalyst decreases the surface area of catalysts if it exists in the surroundings. The deactivation is the main reason of failure of catalytic exterior surface area due to the crystalline development of catalytic phase. The main reason of poisoning is due to the high adsorption of feed impurities as shown in Fig. 27; therefore, poisoned catalysts are very tough to regenerate [116, 117].

Poisoning is highly affected by reactants, products, or impurities present on sites or else existing for the catalysis. Depending over the poisonous concentration, poisoning might be fast or slow; measured on the strong poison

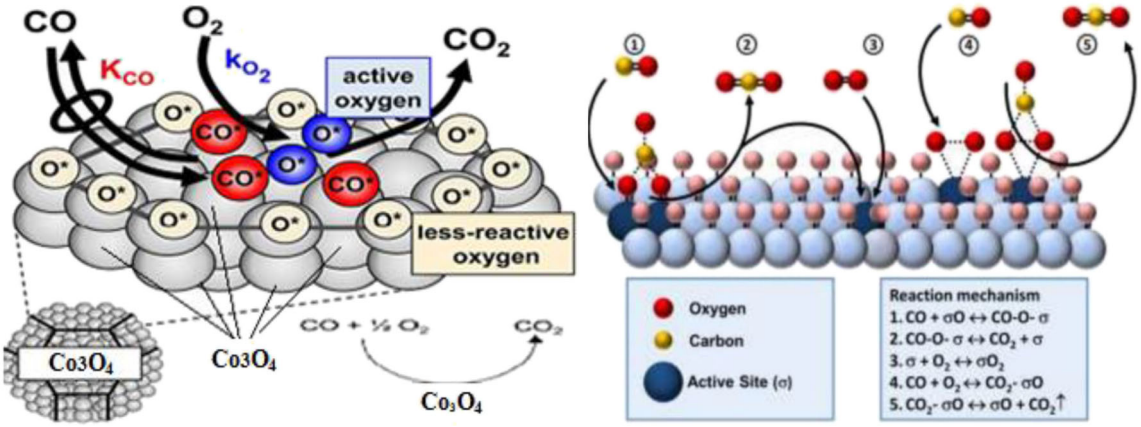

Fig. 18 Mechanism of CO oxidation over transition metal catalyst

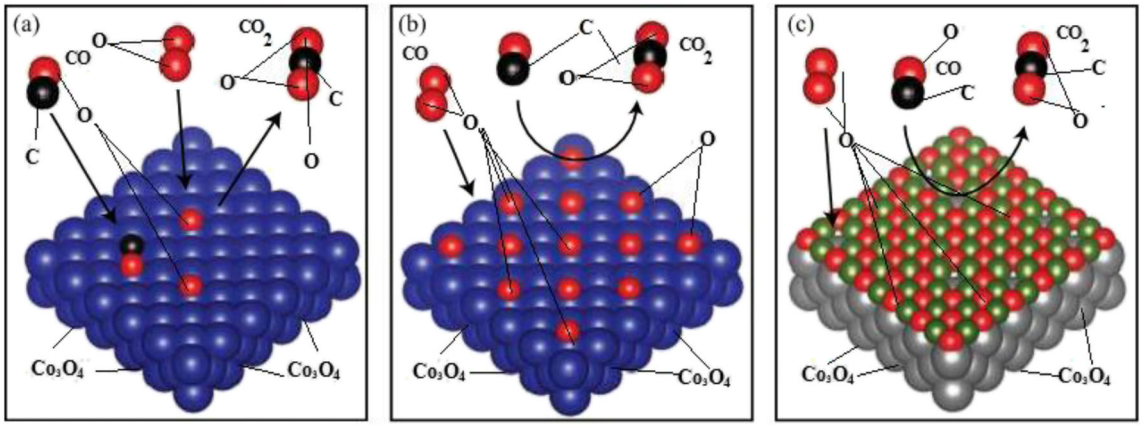

Fig. 19 Illustration of **a** Langmuir-Hinshelwood mechanism, **b** Eley-Rideal mechanism, and **c** Mars-van Krevelen mechanism

adsorption, poisoning is either reversible or irreversible. The current technologies shown for good understanding of deactivation mechanisms that will facilitate more efficient design and optimization of processes concerning deactivating catalysts were available [103–106].

7 Regeneration of transition metal catalysts

The different steps are applied in the regeneration of catalysts were represented in Fig. 28. The activity of reused catalysts mostly depends on catalysts chemical composition and recycling conditions. In general in a reaction cycle, the catalyst follows two main steps: (i) separation from the reaction mixture for catalyst collection and (ii) treatment for its regeneration. The catalysts are recovered by filtration using separation funnel, centrifugation, and sedimentation. Ideally, a catalyst should be reused as numerous times as possible without any treatment. The reusability of catalyst could be done by further treatment for regeneration prior to next use. The strategy for increasing the life and reusability of transition metal catalyst and preparation for catalyst removing with correspond to catalytic converters is noted [118, 119]. The mild drying/calcination in atmosphere increased temperatures to generate catalytically active oxides. In regeneration by the presence of robust washing and chemical treatments to remove channel blockages, deactivated catalyst metals, and poisons, followed by chemical treatments to restore active catalytic materials,

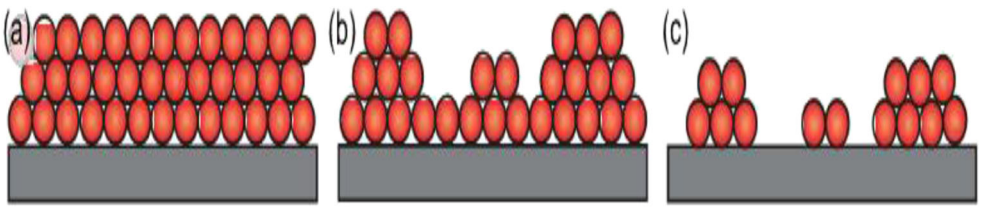

Fig. 20 Illustration of **a** Frank-van der Merwe, **b** Stranski-Krastanov, and **c** Vollmer-Weber

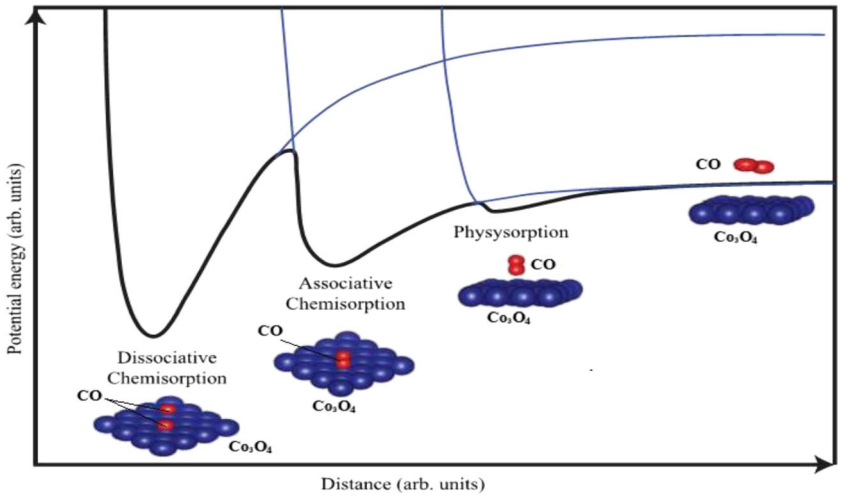

Fig. 21 The potential energy curves of gas adsorption process

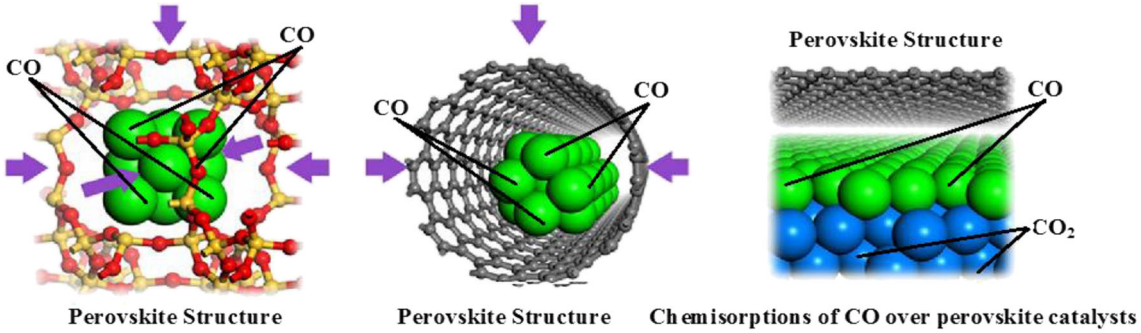

Fig. 22 Mechanism for CO chemisorptions over perovskite catalysts

Fig. 23 Kinetics study of CO adsorptions over transitional metal catalysts

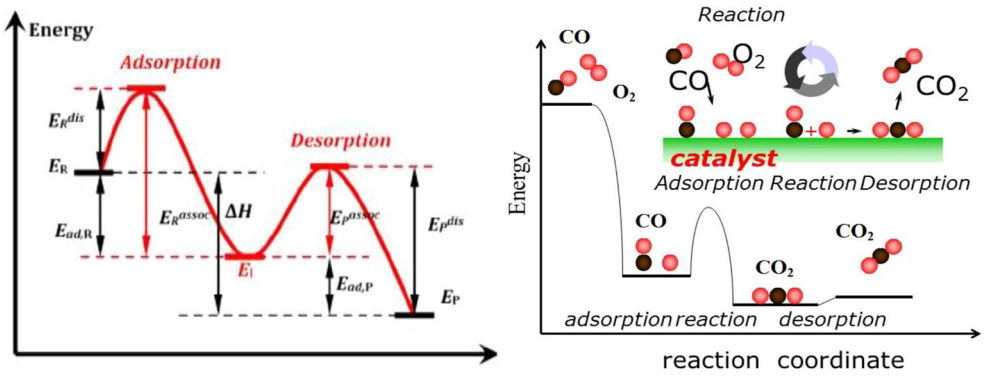

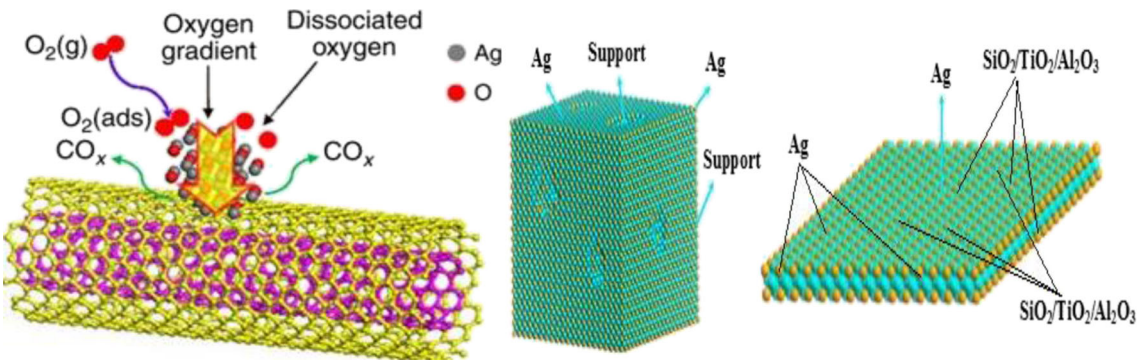

Fig. 24 Mechanism of CO oxidation over transition metal catalyst

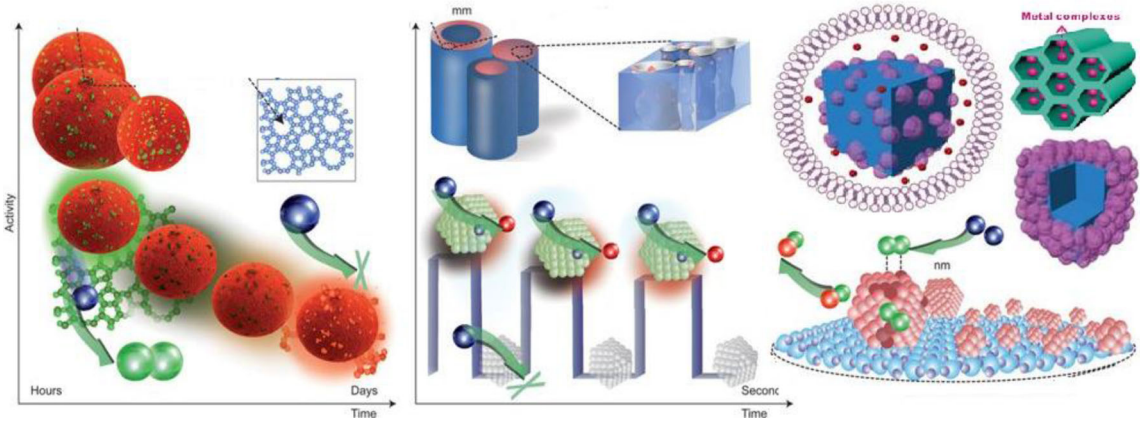

Fig. 25 Deactivation of transition metal catalysts

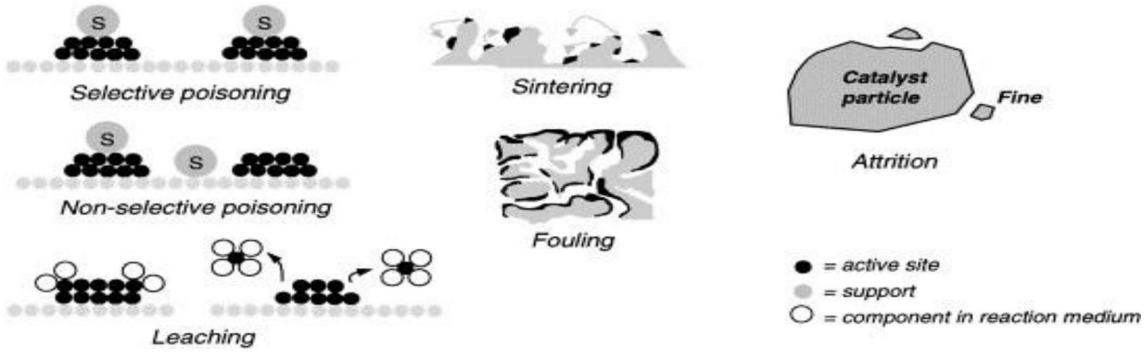

Fig. 26 Deactivation of transition metal catalysts by sintering and fouling

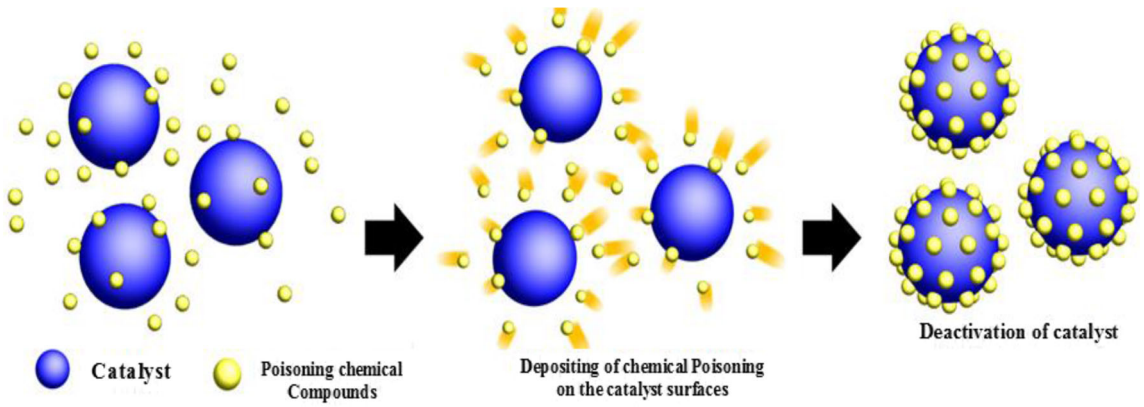

Fig. 27 Deposition of chemical poisoning on the catalysts surfaces

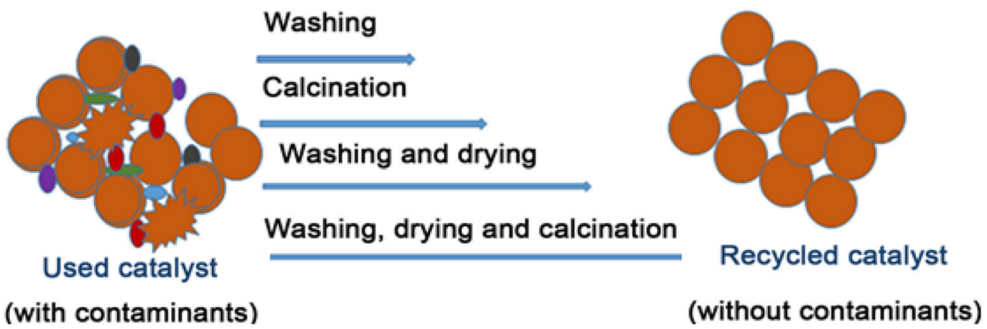

Fig. 28 Regeneration of transition metal catalysts

normal regeneration conditions are considered to elimination of blockages, deactivated catalyst, poisons and restore active catalytic material [120, 121]. The mechanism of catalyst deactivation is more important to the applications of its regeneration process. An economical possibility to preparation of catalyst by decreasing the price of manufacture was shown, and for actual high-scale application, a significant characteristic feature of catalyst is its "reuse" property [122, 123].

The transition metal catalysts regeneration processes are applied for total removing of blinding layers, catalyst performances usually superior after regeneration, SO_2 to SO_3 conversion rate, mechanical constancy, and deactivation rate in all properties of regenerated catalyst are as better than the novel catalyst. The off-site regeneration processes are more sophisticated and demanding than on-site rejuvenation processes; it offer considerably more efficient cleaning and reconstitution of catalyst with complete improvement of activity—sometimes better than the fresh catalyst performances [124]. Rejuvenation showed only partial (up to 85%) recovery of the original activity. The fresh catalyst performs by removing the carbon deposits and returning the sintered transition metal catalyst particles close to the optimum size. The careful estimation of basic causes of TMO catalyst deactivation is significant catalytic system and represents how correct choice of regeneration conditions can improve the life of catalysts by redispersion of active metal. Sintering is most excellently removed by minimizing and controlling the temperature of reaction, even though the new developments have pay attention on encapsulating metal crystallites to remove the mobility, while remain allowing entrance for reactants and products [125–127]. Transition metal catalyst regeneration is possible in various situations in particular to recover activity failure due to fast coking or more term deactivation related with failure of active metal dispersion. Typically, the regeneration or rejuvenation strategies of transition metal catalysts are discussed by the procedure or financial requirement to obtain the certain process on running lengths [128–131]. Life cycle working strategies are essential when operational catalyst regeneration against replacement decisions. Rejuvenation treatments can improve the valuable life of transition metal catalysts. Selective catalytic reduction catalysts showed superior TMO catalysts rejuvenation practiced in a viable process. The regeneration of deactivated catalysts is mostly depending on the chemical, economical, and environmental factors [132–134].

8 Conclusions

Carbon monoxide is a poisonous gas which should be removed from exhaust gases and stationary sources. Catalytic reaction is broadly applied for measuring the catalytic performances of novel materials. The transition metal catalysts are highly prominent metal oxide catalysts for ambient temperature CO oxidation. The clean and reduced transition metal catalysts is needed rather it seems to be accepted that the adsorbed oxygen is required to bring about CO adsorption. The CO oxidation over transition metal catalysts to be associated in the presence of several forms of chemisorbs reactants, products, and intermediates on the surface. The Co_3O_4, Mn_2O_3, Cu_2O, ZnO, NiO, Fe_2O_3, IrO_2, and NiO catalysts are individual one of the most significant TMO catalysts for ambient temperature CO conversion. The accumulation of suitable promoters, supports, pretreatment, and superior preparation methods would result to improvement in the performances of transition metal catalyst toward CO oxidation. The relative ease of preparation, good thermal and chemical stability, and high activity of transition metal catalysts offer better activity for automobile vehicle pollution control applications. This review paper represents an important information about the pure and substituted transition metal catalysts for CO emissions control.

Acknowledgments The authors would like to express his gratitude to the Department of Civil Engineering and Chemical Engineering and Technology, Indian Institute of Technology (Banaras Hindu University) Varanasi, India, for their guidance and support.

Compliance with ethical standards

Conflict of interest There is no conflict of interest.

References

1. Li Z, Wang H, Wu X, Ye Q, Xu X, Li B, Wang F (2017) Novel synthesis and shape-dependent catalytic performance of Cu–Mn oxides for CO oxidation. Appl Surf Sci 403:335–341
2. Dey S, Dhal GC, Prasad R, Mohan D (2016) Effect of nitrate metal (Ce, Cu, Mn and Co) precursors for the total oxidation of carbon monoxide. Res Effi Tech 3:293–302
3. Dey S, Dhal GC, Mohan D, Prasad R (2017) Kinetics of catalytic oxidation of carbon monoxide over CuMnAgOx catalyst. Mater Disc 8:18–25
4. Wu Y, Wang DS, Li YD (2014) Nanocrystals from solutions: catalysts. Chem Soc Rev 43:2112–2124
5. Yuan CZ, Wu HB, Xie Y, Lou XW (2014) Mixed transition-metal oxides: design, synthesis, and energy-related applications. Angew Chem Int 53:1488–1504
6. Dey S, Dhal GC, Mohan D, Prasad R (2017) Study of Hopcalite (CuMnOx) catalysts prepared through a novel route for the oxidation of carbon monoxide at low temperature. Bull Chem React Eng Catal 12(3):393–407
7. Huang WX (2016) Oxide nanocrystal model catalysts. Acc Chem Res 49:520–527
8. Yec CC, Zeng HC (2014) Synthesis of complex nanomaterials via Ostwald ripening. J Mater Chem A 2:4843–4851
9. Dey S, Dhal GC, Mohan D, Prasad R (2017) Characterization and activity of CuMnOx/γ-Al_2O_3 catalyst for oxidation of carbon monoxide. Mater Disc 8:26–34
10. Dey S, Dhal GC, Mohan D, Prasad R, Gupta RN (2018) Cobalt doped CuMnOx catalysts for the preferential oxidation of carbon monoxide. Appl Surf Sci 441:303–316

11. Balikci F, Guldur C (2007) Characterization and CO oxidation activity studies of Co based catalyst. Turk J Chem 31:465–471
12. Dey S, Dhal GC, Mohan D, Prasad R (2018) Low-temperature complete oxidation of CO over various manganese oxide catalysts. Atmos Pollut Res 9:755–763
13. Liu R, Zhao SQ, Zhang MM, Feng F, Shen Q (2015) High interfacial lithium storage capability of hollow porous Mn_2O_3 nanostructures obtained from carbonate precursors. Chem Commun 51:5728–5731
14. Dey S, Dhal GC, Mohan D, Prasad R (2017) Copper based mixed oxide catalysts (CuMnCe, CuMnCo and CuCeZr) for the oxidation of CO at low temperature. Mater Disc 10:1–14
15. Tang WX, Wu XF, Li SD, Shan X, Liu G, Chen YF (2015) Co-nanocasting synthesis of mesoporous Cu–Mn composite oxides and their promoted catalytic activities for gaseous benzene removal. Appl Catal B 162:110–121
16. Dey S, Dhal GC, Prasad R, Mohan D (2016) Total oxidation of CO by CuMnOx catalyst at a low temperature. Int J Sci Eng Res 7(10):1730–1737
17. Dong RT, Wang HL, Zhang Q, Xu XT, Wang F, Li B (2015) Shape-controlled synthesis of Mn_2O_3 hollow structures and their catalytic properties. CrystEngComm 17:7406–7413
18. Dey S, Dhal GC, Mohan D, Prasad R (2018) The choice of precursors in the synthesizing of CuMnOx catalysts for maximizing CO oxidation. Int J Ind Chem 9:199–214
19. Dey S, Dhal GC, Mohan D, Prasad R (2018) Synthesis and characterization of $AgCoO_2$ catalyst for oxidation of CO at a low temperature. Polyhedron 155:102–113
20. Lee S, Gavriilidis A, Pankhurst QA, Kyek A, Wagner FE, Wong PCL, Yeung KL (2001) Effect of drying conditions of Au-Mn co-precipitates for low temperature CO oxidation. J Catal 200:298–308
21. Dey S, Dhal GC, Mohan D, Prasad R (2018) Effect of various metal oxides phases present in CuMnOx catalyst for selective CO oxidation. Mater Disc 12:63–71
22. Xie X, Li Y, Shen W (2005) Co_3O_4 nanorods for low temperature oxidation of carbon monoxide. Chin Acad Sci, Dalian 116023
23. Jansson J, Skoglundh M, Fridell E, Thormählen P (2001) A mechanistic study of low temperature CO oxidation over cobalt oxide. Top Catal 16(17):385–389
24. Jansson J (2000) Low temperature CO oxidation over Co_3O_4/Al_2O_3. J Catal 194:55–60
25. Dey S, Dhal GC, Mohan D, Prasad R (2017) Effects of doping on the performance of CuMnOx catalyst for CO oxidation. Bull Chem React Eng Catal 12(3):370–383
26. Dey S, Dhal GC, Mohan D, Prasad R (2017) Effect of preparation conditions on the catalytic activity of CuMnOx catalysts for CO oxidation. Bull Chem React Eng Catal 12(3):437–451
27. Larsson PO, Berggren H, Andersson A, Augustsson O (1997) Supported metal oxides for catalytic combustion of CO and VOCs emissions: preparation of titania over layers on a macroporous support. Catal Today 35:137–144
28. Cunningham DAH, Kobayashi T, Kamijo N, Haruta M (1994) Influence of dry operating conditions: observation of oscillations and low temperature CO oxidation over Co_3O_4 and Au/Co_3O_4 catalysts. Catal Lett 25:257–264
29. Xia GG, Yin YG, Willis WS, Wang JY, Suib SL (1999) Efficient stable catalysts for low temperature carbon monoxide oxidation. J Catal 185:91–105
30. Wang Y, Zhao Y, Gao Y, Liu D (2008) Origin of the high activity and stability of Co_3O_4 in low temperature CO oxidation. Catal Lett 125:134–138
31. Tuysuz H, Comotti M, Schuth F (2008) Ordered mesoporous Co_3O_4 as highly active catalyst for low temperature CO-oxidation. Chem Commun:4022–4024
32. Dong ZH, Lai XY, Halpert JE, Yang NL, Yi LX, Zhai J, Wang D, Tang ZY, Jiang L (2012) Accurate control of multishelled ZnO hollow microspheres for dye-sensitized solar cells with high efficiency. Adv Mater 24:1046–1049
33. Royer S, Duprez D (2011) Catalytic oxidation of carbon monoxide over transition metal oxides. Chem Cat Chem 3:24–65
34. Prasad R, Singh P (2013) A novel route of single step reactive calcinations of copper salts far below their decomposition temperatures for synthesis of highly active catalysts. Catal Sci Technol 3:3326–3334
35. Tan Z, Tan H, Shi X, Ji Z, Yan Y, Zhou Y (2015) Metal-organic framework MIL-53(Al)-supported copper catalyst for CO catalytic oxidation reaction. J Inorg Chem Commun 61:128–131
36. Lin H, Chen Y, Wang W (2005) Preparation of nanosized iron oxide and its application in low temperature CO oxidation. J Nano Part Res 7:249–263
37. Swislocki S, Stowe K, Maier WF (2014) Catalysts for selective propane oxidation in the presence of carbon monoxide: mechanistic aspects. J Catal 316:219–230
38. Kwon SC, Fan M, Wheelock TD, Saha B (2007) Nano- and micro-iron oxide catalysts for controlling the emission of carbon monoxide and methane. Sep Purif Technol 58:40–48
39. Cao J, Li G, Wang Y, Sun G, Wang X, Hari B, Zhang Z (2014) Mesoporous Co-Fe-O nanocatalysts: preparation, characterization and catalytic carbon monoxide oxidation. J Environ Chem Eng 2:477–483
40. Gao F, Wang Y, Cai Y, Goodman DW (2009) CO oxidation over Ru (0001) at near-atmospheric pressures: from chemisorbed oxygen to RuO_2. J Surf Sci 603:1126–1134
41. Snytnikov PV, Sobyanin VA, Belyaev VD, Tsyrulnikov PG, Shitova NB, Shlyapin DA (2003) Selective oxidation of carbon monoxide in excess hydrogen over Pt-, Ru- and Pd- supported catalysts. Appl Catal A Gen 239:149–156
42. Haruta M, Yamada N, Kobayashi T, Lijiama S (1989) Gold catalysts prepared by co-precipitation for low-temperature oxidation of hydrogen and of carbon monoxide. J Catal 115:301–309
43. Cole KJ, Carley AF, Crudace MJ, Clarke M, Taylor SH, Hutchings GJ (2010) Copper manganese oxide catalysts modified by gold deposition: the influence on activity for ambient temperature carbon monoxide oxidation. Catal Lett 138:143–147
44. Dey S, Dhal GC, Mohan D, Prasad R (2019) Synthesis of silver promoted CuMnOx catalyst for ambient temperature oxidation of carbon monoxide. J Sci: Adv Mater Devices 4:47–56
45. Cao X, Chen M, Ma J, Yin B, Xing X (2017) CO oxidation by the atomic oxygen on silver clusters: structurally dependent mechanisms generating free or chemically bonded CO_2. Phys Chem Chem Phys 19(1):196–203
46. Abu Bakar WAW, Toemen RAS (2012) Catalytic methanation reaction over supported nickel–ruthenium oxide base for purification of simulated natural gas. Sci Iran 19(3):525–534
47. Hashemnejad SM, Parvari M (2011) Deactivation and regeneration of nickel-based catalysts for steam-methane reforming. Chin J Catal 32(2):273–279
48. Grillo F, Natile MM, Glisenti A (2004) Low temperature oxidation of carbon monoxide: the influence of water and oxygen on the reactivity of a Co_3O_4 powder surface. Appl Catal B Environ 48:267–274
49. Kraum M, Baerns M (1999) Fischer–Tropsch synthesis: the influence of various cobalt compounds applied in the preparation of supported cobalt catalysts on their performance. Appl Catal A Gen 186:189–200
50. Toniolo FS, Schmal M (2016) Improvement of catalytic performance of perovskites by partial substitution of cations and supporting on high surface area materials. Chapter 18, Intech Open Science, https://doi.org/10.5772/61279

51. Kucharczyk B (2015) Catalytic oxidation of carbon monoxide on Pd-containing $LaMnO_3$ perovskites. Catal Lett 145(16):1237–1245
52. Mankidy BD, Balakrishnan N, Joseph B, Gupta VK (2014) CO oxidation by cobalt oxide: an experimental study on the relationship between nanoparticle size and reaction kinetics. J Austin Chem Eng 1:1–6
53. Lin H, Chiu H, Tsai C, Chien S, Wang C (2003) Synthesis, characterization and catalytic oxidation of carbon monoxide over cobalt oxide. Catal Lett 88:169–174
54. Ilton ES, Post JE, Heaney PJ, Ling FT, Kerisit SN (2016) XPS determination of Mn oxidation states in Mn (hydr)oxides. Appl Surf Sci 366:475–485
55. Manceau A, Marcus MA, Grangeon S (2012) Determination of Mn valence states in mixed-valent manganates by XANES spectroscopy. Am Mineral 97(6):816–827
56. Villalobos M, Toner B, Bargar J, Sposito G (2003) Characterization of the manganese oxide produced by *Pseudomonas putida* strain MnB1. Geochim Cosmochim Acta 67(14):2649–2662
57. Muralidhara K, Misra P (2014) A study on the surface properties of transition metal oxides. Int J Sci Res Manag 2(12):1880–1883
58. Stancheva M, Manev S, Lazarov D, Mitov M (1996) Catalytic activity of nickel based amorphous alloys for oxidation of hydrogen and carbon monoxide. Appl Catal A Gen 135:19–24
59. Larsson P, Andersson A, Wallenberg LR, Svensson B (1996) Combustion of CO and toluene: characterization of copper oxide supported on titania and activity comparisons with supported gold, iron and manganese oxide. J Catal 163:279–293
60. Al-Sayari S, Carley CF, Taylor SH, Hutchings GJ (2007) Au/ZnO and Au/Fe_2O_3 catalysts for CO oxidation at ambient temperature: comments on the effect of synthesis conditions on the preparation of high activity catalysts prepared by Co precipitation. Top Catal 44(1-2):123–128
61. Bordoloi A, Sanchez M, Noei H, Kaluza S, Grobmann D, Wang Y, Grunert W, Muhler M (2014) Catalytic behavior of mesoporous cobalt-aluminum oxides for CO oxidation. J Catal 45:1–9
62. Xanthopoulou G, Vekinis G (1998) Investigation of catalytic oxidation of carbon monoxide over a Cu±Cr-oxide catalyst made by self-propagating high-temperature synthesis. Appl Catal B Environ 19:37–44
63. Luo M, Fang P, He M, Xie Y (2005) In situ XRD, Raman, and TPR studies of CuO/Al_2O_3 catalysts for CO oxidation. J Mol Catal A Chem 239:243–248
64. Pelardy F, Daudin A, Devers E, Dupont C, Raybaud P, Brunet S (2016) Deep HDS of FCC gasoline over alumina supported CoMoS catalyst: inhibiting effects of carbon monoxide and water. Appl Catal B Environ 183:317–327
65. Hernanndez WY, Centeno MA, Romero-Sarria F, Ivanova S, Montes M, Odriozola JA (2010) Modified cryptomelane-type manganese dioxide nanomaterials for preferential oxidation of CO in the presence of H_2. Catal Today 157:160–165
66. Cao J, Li G, Wang Y (2015) Oil shale ash supported CuO nanocatalysts: preparation, characterization and catalytic activity for CO oxidation. J Environ Chem Eng 3:1725–1730
67. Deng S, Xiao X, Xing X, Wu J, Wen W, Wang Y (2015) Structure and catalytic activity of 3D macro/mesoporous Co_3O_4 for CO oxidation prepared by a facile self-sustained decomposition of metal organic complexes. J Mol Catal A Chem 398:79–85
68. Li P, Miser DE, Rabiei S, Yadav RT, Hajaligol MR (2003) The removal of carbon monoxide by iron oxide nanoparticles. Appl Catal B Environ 43:151–162
69. Loaiza-Gil A, Fontal B, Rueda F, Mendialdua J, Casanova R (1999) On carbonaceous deposit formation in carbon monoxide hydrogenation on a natural iron catalyst. Appl Catal A Gen 177:193–203
70. Sun S, Gao Q, Wang H, Zhu J, Guo H (2010) Influence of textural parameters on the catalytic behavior for CO oxidation over ordered mesoporous Co_3O_4. Appl Catal B Environ 97:284–291
71. Huang T, Lee K, Yang H, Dow W (1998) Effect of chromium addition on supported copper catalysts for carbon monoxide oxidation. Appl Catal A Gen 174:199–206
72. Dehestaniathar S, Khajelakzay M, Ramezani-Farani M, Ijadpanah-Saravi H (2015) Modified diatomite-supported CuO-TiO_2 composite: preparation, characterization and catalytic CO oxidation. J Taiwan Inst Chem Eng:1–7
73. Qwabe LQ, Friedrich HB, Singh S (2015) Preferential oxidation of CO in a hydrogen rich feed stream using Co-Fe mixed metal oxide catalysts prepared from hydrotalcite precursors. J Mol Catal A Chem 404:167–177
74. Salek G, Alphonse P, Dufour P, Guillemet-Fritsch S, Tenailleau C (2014) Low temperature carbon monoxide and propane total oxidation by nanocrystalline cobalt oxides. Appl Catal B Environ 147:1–7
75. Halim KSA, Khedr MH, Nasr MI, El-Mansy AM (2007) Factors effecting CO oxidation over nanosized Fe_2O_3. Mater Res Bull 42:731–741
76. Tang Y, Dong L, Deng C, Huang M, Li B, Zhang H (2016) In-Situ FTIR investigation of CO oxidation on CuO/TiO_2 catalyst. Catal Commun 28:1–17
77. Zhu J, Zhao Z, Xiao D, Li J, Yang X, Wu Y (2005) CO oxidation, NO decomposition, and NO + CO reduction over perovskite-like oxides La_2CuO_4 and $La_{2-X}Sr_XCuO_4$: an MS-TPD study. Ind Eng Chem Res 44(12):4227–4233
78. Liu Y, Dai H, Du Y, Deng J, Zhang L, Zao Z, Au CT (2012) Controlled preparation and high catalytic performance of three-dimensionally ordered macroporous $LaMnO_3$ with nanovoid skeletons for the combustion of toluene. J Catal 287:149–160
79. Kim MH, Kim DW (2011) Parametric study on the deactivation of supported Co_3O_4 catalysts for low temperature CO oxidation. Chin J Catal 32:762–770
80. Yung MM, Holmgreen EM, Ozkan US (2007) Low-temperature oxidation of carbon monoxide on Co/ZrO_2. Catal Lett 118:180–186
81. Liu C, Virginie M, Constant A, Khodakov A (2015) Impact of potassium content on the structure of molybdenum nanophases in alumina supported catalysts and their performance in carbon monoxide hydrogenation. Appl Catal A Gen 504:565–575
82. Pollard MJ, Weinstock BA, Bitterwolf TE, Griffiths PR, Newbery AP, Paine JB (2008) A mechanistic study of the low temperature conversion of carbon monoxide to carbon dioxide over a cobalt oxide catalyst. J Catal 254:218–225
83. Feyzi M, Khodaei MM, Shahmoradi J (2015) Preparation and characterization of promoted Fe-Mn/ZSM-5 nano catalysts for CO hydrogenation. Int J Hydrog Energy 40:14816–14825
84. Zhang Y, Chen Y, Zhou J, Wang T, Zhao Y (2009) Synthesis and high catalytic activity of mesoporous Co_3O_4 nanowires for carbon monoxide oxidation. Solid State Commun 149:585–588
85. Cao J, Wang Y, Yu X, Wang S, Wu S, Yuan Z (2008) Mesoporous CuO–Fe_2O_3 composite catalysts for low-temperature carbon monoxide oxidation. Appl Catal B Environ 79:26–34
86. Li J, Li L, Wu F, Zhang L, Liu X (2013) Dispersion-precipitation synthesis of nanorod Mn_3O_4 with high reducibility and the catalytic complete oxidation of air pollutants. Catal Commun 31:52–56
87. Umegaki T, Inoue T, Kojima Y (2016) Fabrication of hollow spheres of Co_3O_4 for catalytic oxidation of carbon monoxide. J Alloys Compd 663:68–76
88. Amini E, Rezaei M (2015) Preparation of mesoporous Fe-Cu mixed metal oxide nanopowder as active and stable catalyst for low temperature CO oxidation. Chin J Catal 36:1711–1718

89. Du Y, Meng Q, Wang J, Yan J, Fan H, Liu Y, Dai H (2012) Three dimensional mesoporous manganese oxides and cobalt oxides: high efficiency catalysts for the removal of toluene and carbon monoxide. J Microporous Mesoporous Mater 162:199–206
90. Wu T, Yan Q, Wan H (2005) Partial oxidation of methane to hydrogen and carbon monoxide over Ni/TiO_2 catalysts. J Mol Catal A Chem 226:41–48
91. Fazlollahi F, Sarkari M, Gharebaghi H, Atashi H, Zarei MM, Mirzaei AA, Hecker WC (2013) Preparation of Fe-Mn/K/Al_2O_3 Fischer-Tropsch catalyst and its catalytic kinetics for the hydrogenation of carbon monoxide. Catal Kinet React Eng 21:507–519
92. Snapkauskiene V, Valincius V, Valatkevicius P (2011) Experimental study of catalytic CO oxidation over CuO/Al_2O_3 deposited on metal sheets. Catal Today 176:77–80
93. Hu C, Gao Z, Yang X (2007) Facile synthesis of single crystalline a-Fe_2O_3 ellipsoidal nanoparticles and its catalytic performance for removal of carbon monoxide. Mater Chem Phys 104:429–433
94. Park PW, Ledford JS (1998) The influence of surface structure on the catalytic activity of alumina supported copper oxide catalysts oxidation of carbon monoxide and methane. Appl Catal B Environ 15:221–231
95. Wang Y, Zhu X, Crocker M, Chen B, Shi C (2014) A comparative study of the catalytic oxidation of HCHO and CO over $Mn_{0.75}Co_{2.25}O_4$ catalyst: the effect of moisture. Appl Catal B Environ 161:542–551
96. Podyachea OY, Stadnichenko AI, Yashnik SA, Stonkus OA, Slavinskaya EM, Boronin AI, Puzynin AV, Ismagilov ZR (2014) Catalytic and capacity properties of nano composites based on cobalt oxide and nitrogen-doped carbon nanofibers. Chin J Catal 35:960–969
97. Chien C, Chuang W, Huang T (1995) Effect of heat treatment conditions on Cu-Cr/γ-alumina catalyst for carbon monoxide and propane oxidation. Applied Catalysis A : General 131:73–87
98. Biabani-Ravandi A, Rezaei M, Fattah Z (2013) Study of Fe-Co mixed metal oxide nanoparticles in the catalytic low temperature CO oxidation. Process Saf Environ Prot 91:489–494
99. Lv J, Ma X, Bai S, Huang C, Li Z, Gong J (2011) Hydrogenation of carbon monoxide over cobalt nanoparticle supported on carbon nanotubes. Int J Hydrog Energy 36:8365–8372
100. Tyurkin YV, Luzhkova EN, Pirogova GN, Chesalov LA (1997) Catalytic oxidation of CO and hydrocarbons on SHS prepared complex metal oxide catalysts. Catal Today 33:191–197
101. Alvarez A, Ivanova S, Centeno MA, Odriozola JA (2012) Sub-ambient CO oxidation over mesoporous Co_3O_4: effect of morphology on its reduction behavior and catalytic performance. Appl Catal A Gen 431:9–17
102. Khedr MH, Halim KSA, Nasr MI, El-Mansy AM (2006) Effect of temperature on the catalytic oxidation of CO over nano-sized iron oxide. Mater Sci Eng A 430:40–45
103. Yunbo Y, Jiaojiao Z, Xue H, Yan Z, Xiubo Q, Baoyi W (2013) Influence of calcinations and pretreatment conditions on the activity of Co_3O_4 for CO oxidation. Chin J Catal 34:283–293
104. Nagase K, Zheng Y, Kodama Y, Kakuta J (1999) Dynamic study of the oxidation state of copper in the course of carbon monoxide oxidation over powdered CuO and Cu_2O. J Catal 187:123–130
105. Konova P, Stoyanova M, Naydenov A, Christoskova S, Mehandjiev D (2006) Catalytic oxidation of VOCs and CO by ozone over alumina supported cobalt oxide. Appl Catal A Gen 298:109–114
106. Wagloehner S, Reichert D, Leon-Sorzano D, Balle P, Geiger B, Kureti S (2008) Kinetic modeling of the oxidation of CO on Fe_2O_3 catalyst in excess of O_2. J Catal 260:305–314
107. Kasmi AE, Tian Z, Vieker H, Beyer A, Chafik T (2016) Innovative CVD synthesis of Cu_2O catalysts for CO oxidation. Appl Catal B Environ 186:10–18
108. Guo MY, Liu F, Tsui J, Voskanyan AA, Ng AMC, Djurisic AB, Chan WK, Chan W, Liao C, Shih K, Surya C (2015) Hydrothermally synthesized Cu_XO as a catalyst for CO oxidation. J Mater Chem 3:3627–3632
109. Huang T, Tsai D (2003) CO oxidation behavior of copper and copper oxide. Catal Lett 87:173–178
110. Dow W, Huang T (1996) Yttria stabilized zirconia supported copper oxide catalyst. J Catal 160:71–182
111. White B, Yin M, Hall A, Le D, Stolbov S, Rahman T, Turro N, O'Brien S (2006) Complete CO oxidation over Cu_2O nanoparticles supported on silica gel. Nano Lett 6:2095–2098
112. Rattan G, Kaur R (2015) Total oxidation of CO using Cu & Co catalyst: kinetic study and calcinations effect. Bull Chem React Eng Catal 10(3):281–293
113. Chen CS, Chen TC, Chen CC, Lai YT, You JH, Chou TM, Chen CH, Lee J (2012) Effect of Ti^{3+} on TiO_2 supported Cu catalysts used for CO oxidation. ACS Lang 28:9996–10006
114. Li B, Wei Y, Wang H (2014) Non-isothermal reduction kinetics of Fe_2O_3-NiO composites for formation of Fe-Ni alloy using carbon monoxide. Trans Nonferrous Metals Soc China 24:3710–3715
115. Zhang Y, Wu Y, Wang H, Guo Y, Wang L, Zhan W, Guo Y, Lu G (2015) The effect of the presence of metal Fe in the CO oxidation over Ir/FeOx catalyst. Catal Commun 61:83–87
116. Zhao Z, Li Y, Bao T, Wang G, Muhammad T (2014) Hierarchically nanoporous Co-Mn-O/FeOx as a high performance catalyst for CO preferential oxidation in H_2-rich stream. Catal Commun 46:28–31
117. Dey S, Dhal GC (2019) Applications of silver nanocatalysts for low-temperature oxidation of carbon monoxide. Inorg Chem Commun 110(107614):1–12
118. Dey S, Dhal GC (2019) A review of synthesis, structure and applications in hopcalite catalysts for carbon monoxide oxidation. Aerosol Sci Eng. https://doi.org/10.1007/s41810-019-00046-1
119. Dey S, Dhal GC (2019) Materials progress in the control of CO and CO_2 emission at ambient conditions: an overview. Mater Sci Energy Technol 2:607–623
120. Punde SS, Tatarchuk BJ (2012) Microfibrous entrapped catalysts for low temperature CO oxidation in humid air. Catal Commun 27: 9–12
121. Védrine JC (2017) Heterogeneous catalysis on metal oxides. Catalysts 7:341–365
122. Musick JK, Williams FW (1975) Hopcalite catalyst for catalytic oxidation of gases and aerosols. Ind Eng Chem Prod Res Dev 14(4):284–286
123. Guo Y, Li C, Lu S, Zhao C (2016) Low temperature CO catalytic oxidation and kinetic performances of KOH–hopcalite in the presence of CO_2. RSC Adv 6:7181–7188
124. Szynkowska M, Węglińska A, Wojciechowska E, Paryjczak T (2009) Oxidation of thiophene over copper-manganese mixed oxides. Chem Pap 63(2):233–238
125. Soliman NK (2019) Factors affecting CO oxidation reaction over nanosized materials: a review. J Mater Res Technol 8(2):2395–2407
126. Ivanov KI, Kolentsova EN, Dimitrov DY, Petrova PT, Tabakova TT (2015) Alumina supported Cu-Mn-Cr catalysts for CO and VOCs oxidation. Int J Mater Metall Eng 9(5):651–658
127. Wegrzyniak A, Jarczewski S, Wegrzynowicz A, Michorczyk B, Ku´strowski P, Michorczyk P (2017) Catalytic behavior of chromium oxide supported on nanocasting-prepared mesoporous alumina in dehydrogenation of propane. Nanomaterials 7(249):1–16
128. Michorczyk P, Ogonowski J, Kus´trowski P, Chmielarz L (2008) Chromium oxide supported on MCM-41 as a highly active and selective catalyst for dehydrogenation of propane with CO_2. Appl Catal A Gen 349:62–69

129. Zhang X, Yue Y, Gao Z (2002) Chromium oxide supported on mesoporous SBA-15 as propane dehydrogenation and oxidative dehydrogenation catalysts. Catal Lett 83:19–25
130. Cherian M, Rao MS, Yang WT, Jehng JM, Hirt AM, Deo G (2002) Oxidative dehydrogenation of propane over Cr_2O_3/Al_2O_3 and Cr_2O_3 catalysts: effects of loading, precursor and surface area. Appl Catal A Gen 233:21–33
131. Ye Z, Giraudon JM, Geyter ND, Morent R, Lamonier JF (2018) The design of MnOx based catalyst in post-plasma catalysis configuration for toluene abatement. Catalysts 8(2):91. https://doi.org/10.3390/catal8020091
132. Dey S, Dhal GC, Mohan D, Prasad R (2019) Application of hopcalite catalyst for controlling carbon monoxide emission at cold-start emission conditions. J Traffic Transp Eng (English Edition). https://doi.org/10.1016/j.jtte.2019.06.002
133. Bonanni S, Ait-Mansour K, Harbich W, Brune H (2012) Effect of the TiO_2 reduction state on the catalytic CO oxidation on deposited size-selected Pt clusters. J Am Chem Soc 134(7):3445–3450
134. Wang S, Yang Z, Chu X, Wang W (2018) Design of efficient catalysts for CO oxidation on titanium carbide–supported platinum via computational study. J Phys Chem C. https://doi.org/10.1021/acs.jpcc.8b0774
135. Roy M, Basak S, Naskar MK (2016) Bi-template assisted synthesis of mesoporous manganese oxide nanostructures: tuning properties for efficient CO oxidation. RSC, Phys Chem Chem Phys 18:5253–5263
136. Han SW, Kim DH, Jeong M, Park KJ, Kim YD (2016) CO oxidation catalyzed by NiO supported on mesoporous Al_2O_3 at room temperature. Chem Eng J 283:992–998
137. Wenge Q, Yu W, Chuanqiang L, Zongcheng Z, Xuehong Z, Guizhen Z, Rui W, Hong H (2012) Effect of activation temperature on catalytic performance of CuBTC for CO oxidation. Chin J Catal 33:986–992
138. Cheng T, Fang Z, Hu Q, Han K, Yang X, Zhang Y (2007) Low temperature CO oxidation over CuO/Fe_2O_3 catalysts. Catal Commun 8:1167–1171
139. Szegedi A, Hegedu M, Margitfalvi JL, Kiricsi I (2004) Low temperature CO oxidation over iron-containing MCM-41 catalysts. Chem Commun:1441–1443
140. Zhu B, Zhang X, Wang S, Zhang S, Wu S, Huang W (2007) Synthesis and catalytic performance of TiO_2 nanotubes-supported copper oxide for low temperature CO oxidation. Microporous Mesoporous Mater 102:333–336
141. Li J, Li L, Cheng W, Wu F, Lu X, Li Z (2014) Controlled synthesis of diverse manganese oxide based catalysts for complete oxidation of toluene and carbon monoxide. Chem Eng J 244:59–67
142. Maity A, Ghosh A, Majumder SB (2016) Engineered spinel-perovskite composite sensor for selective carbon monoxide gas sensing. J Sensors Actuators B Chem 15:1–23
143. Zhou R, Jiang X, Mao J, Zheng X (1997) Oxidation of carbon monoxide catalyzed by copper-zirconium composite oxides. Appl Catal A Gen 162:213–222
144. Pakharukova VP, Moroz EM, Kriventsov VV, Zyuzin DA, Kosmambetova GR, Strizhak PE (2009) Copper-cerium oxide catalysts supported on monoclinic zirconia: structural features and catalytic behavior in preferential oxidation of carbon monoxide in hydrogen excess. Appl Catal A Gen 365:159–164
145. Singh S, Madras G (2015) Detailed mechanism and kinetic study of CO oxidation on cobalt oxide surfaces. Appl Catal A Gen 504:463–475
146. Kuo CH (2015) Design, synthesis, and characterization of transition metal oxide based functional materials for multi-phase catalytic applications. University of Connecticut Graduate School, Taiwan
147. Balakrishnan N (2013) Theoretical studies of Co based catalysts on CO hydrogenation and oxidation. University of South Florida Scholar Commons, Florida
148. Binder AJ (2015) Synthesis and characterization of support modified nanoparticle-based catalysts and mixed oxide catalysts for low temperature CO oxidation. University of Tennessee, Knoxville
149. Prasad R, Singh P (2012) A review on CO oxidation over copper chromite catalyst. Catal Rev 54(2):224–279
150. Rajska M, Długosz P, Zybała R (2016) Effect of support structure in Au/Al_2O_3-TiO_2 catalysts in low-temperature CO oxidation. SEED, E3S Web of Conferences, 10, 00131, DOI: https://doi.org/10.1051/2016E3S.
151. Lee DS, Chen YW (2013) Synthesis of CoOx-TiO_2 catalysts and its application for low-temperature CO oxidation. J Catal 586364:1–9. https://doi.org/10.1155/2013/586364
152. Park NK, Lee YJ, Kwon BC, Lee TJ, Kang SH, Hong BU, Kim T (2019) Optimization of nickel-based catalyst composition and reaction conditions for the prevention of carbon deposition in toluene reforming. Energies 12:1307. https://doi.org/10.3390/en12071307
153. Yi Y, Zhang P, Qin Z, Yu C, Li W, Qin Q, Li B, Fan M, Lianga X, Dong L (2018) Low temperature CO oxidation catalysed by flower-like Ni–Co–O: how physicochemical properties influence catalytic performance. RSC Adv 6:7110–7122
154. Parravano G (1953) The catalytic oxidation of carbon monoxide on nickel oxide II. Nickel oxide containing foreign ions. J Am Chem Soc 75(6):1452–1454. https://pubs.acs.org/doi/10.1021/ja01102a051
155. Saber O, Zaki T (2014) Carbon monoxide oxidation using Zn–Cu–Ti hydrotalcite-derived catalysts. J Chem Sci 126(4):981–988
156. Gac W, Zawadzki W, Słowik G, Greluk M, Pawlonka J, Machocki A (2016) Chromium-modified zinc oxides. J Therm Anal Calorim 125:1205–1215
157. Chafidz A, Megawati, Widyastuti CR, Augustia V, Nisa K, Ratnaningrum (2018) Application of copper-zinc metal as a catalytic converter in the motorcycle muffler to reduce the exhaust emissions. Int Con Env Sc Eng (8th) 167:1–8
158. Allam D, Bennici S, Limousy L, Hocine S (2019) Improved Cu- and Zn-based catalysts for CO_2 hydrogenation to methanol. Comptes Rendus Chim 22:227–237
159. Jiajian G, Jia C, Li J, Zhang M (2013) Ni/Al_2O_3 catalysts for CO methanation: effect of Al_2O_3 supports calcined at different temperatures. J Energy Chem 22(6):919–927